UNIVERISTY OF OXFORD

FINAL HONOUR SCHOOL OF ENGINEERING SCIENCE

FOURTH YEAR PROJECT

Modelling the Dementia Brain

Author:

Timothy STUART

Oriel College

Supervisor:

Dr. Stephen PAYNE

Acknowledgments

I would like to express my considerable gratitude to Dr Stephen Payne, my supervisor, for his patient guidance, valuable insights and his creation of a fascinating project. His willingness to give time remotely so generously has been greatly apprenticed during the challenge of COVID-19.

Abstract

Alzheimer's dementia's (AD) economic and social cost increases yearly and countries with aging populations are the most severely affected. Little is known for certain about the causes of this disease. Put forward in 1991, the amyloid cascade hypothesis has garnered the most attention, but positive clinical results remain lacking. Innovative methods and new research avenues are therefore needed to investigate AD.

Changes in blood flow have long been linked to AD pathology. Hypoperfusion has been shown to precede other AD symptoms and AD patients often suffer cerebrovascular diseases. However, further modelling is needed to gain insight to the exact nature of their relationship. New research has recognised the pivotal role of the neurovascular unit and the pericytes' response in microvasculature blood flow. This project attempts to computationally model and measure the effect of the pericytes' response on AD.

To do so, it adapts the vascular anatomical network, an existing microvasculature network and flow model from Payne (2018) [1]. New contributions are the inclusion of pericytes' response to flow reduction and mass action kinetics style health models. To solve these, a Runge-Kutta fourth order numerical solver is used.

The findings of this report reflect the importance of pericyte death on blood flow and amyloid beta accumulation in the brain. Interestingly, it also shows that rapid neuron death halts the death of pericytes and even restores them, suggesting that neurons may be sacrificed to protect the health of pericytes. Due to computational resource and time restraints, the maximum duration of simulations run was 2400 s. However, the project demonstrates the possibility and potential value of simulation durations in the order of realistic AD development.

Contents

1 Nomenclature

Variables

p	Static pressure
p_t	Tisse partial pressure of oxygen
p_b	Blood partial pressure of oxygen
$\hat{p}_t$	Volume averaged tissue partial pressure of oxygen
Q	Flow rate
R	Resistance to flow
t	Time
μ	Dynamic viscosity of blood
c	Concentration of amyolid beta
L	Length of vessel
D	Diameter
α_t	Solubility coefficient of oxygen in brain tissue
V_t	Volume of vessel tissue compartment
V_b	Volume of blood in vessel
K	Oxygen permeability of vascular wall
h	Vessel wall thickness
M	Oxygen consumption rate of tissue per unit volume
S	Saturation of oxygen in blood
$c_{H,b}$	Oxygen-carrying capacity per unit volume of red blood cells
H	Hematocrit
ϕ	Normalised diameter of capillary bed
ϕ_{min}	Scaling factor for pericyte response
α	Proportion of pericytes responding to flow rate changes
A	Alive proportion
V	Vulnerable proportion
D	Dead proportion
k	Rate
τ_d	Pericyte response delay
τ_p	Pericyte response time constant
τ_c	AB accumulation time constant

Subscripts/Superscripts

p	Relating to pericytes
n	Relating to neurons
+	Forward in the health models
-	Backward in the health models

Abbreviations

NVU	Neurovascular unit
AD	Alzheimer's dementia
CVD	Cerebrovascular disease
AB	Amyloid Beta
ADP	Cerebrovascular pathology
CVP	Alzheimer's dementia pathology

2 Introduction

Dementia is a progressive degenerative disease culminating in severe brain dysfunction. It is now the fifth biggest killer worldwide [2], yet relatively little is known about the disease compared to the other major killers. Alzheimer's Disease (AD) is the most common form of dementia and therefore is the most pressing to solve. The most prevalent theory of the cause of AD is the amyloid cascade hypothesis, which holds that the amyloid β protein (AB), which appears to build-up as plaques in all AD brains, is the causative agent of the AD pathology. Despite positive expectations, little headway has been made on the treatment and prevention of AD, with failure after failure of drugs aimed at tackling this amyloid cascade issue. Therefore, in recent times there has been a push to explore alternative actors in the onset of AD.

The relationship between vascular factors and AD has been well documented, but little investigation has been conducted in the role that blood flow may play in causing AD pathology. The neurovascular unit (NVU) over the last two decades has received increasing attention as more data suggests its importance in microvasculature blood flow. Pericytes in particular, a constituent of the NVU, have offered feedback loops for microvasculature control and effect, presenting a new line of AD study. This project aims to adapt an existing model of the human microvasculature with a novel pericyte control model to quantitatively show the pericytes' effect on AD and gain insight into the processes that lead to AD. The subsequent results have shown the importance of the pericytes' contraction and death to the accumulation of AB and the death of neurons in the brain, confirming the probability of such a link and paving the way for further modelling and research.

The report will firstly perform a review into relevant literature by explaining the importance and cost of dementia to society, outlining the promising evidence of blood flow and particularly pericytes' importance in AD pathology and briefly introducing the network and model. Next, the model development section details the existing 1-D network and flow model, before addressing the addition of novel methods and their place in this modified flow model. The results section will present simulations of these individual models followed by characteristic responses for the full model and a discussion of these simulations. Finally, a review of some of the issues encountered in the project is undertaken followed by the conclusion and suggestions for future work.

3 Literature Review

A review of current literature was undertaken. It begins by explaining the most important elements of dementia disease, as well as the reasons why much work and research in this field are needed. It will then explore the role that blood flow plays in the dementia puzzle and highlight how recent studies on pericytes have shown that they are highly significant in terms of the cerebral vascular response. Finally, current methods of modelling blood flow are evaluated in addition to highlighting their use in helping to understand the disease better.

3.1 The Importance of Dementia

'Dementia' describes a set of symptoms. This set may include memory loss and difficulties with problem-solving, language and thinking, interfering with individuals' ability to engage in daily life. Despite age being the strongest known risk factor contributing to the onset of dementia, it is not an inevitable consequence of ageing - 9% of the estimated 50 million cases worldwide are young-onsets (defined as cases with individuals experiencing symptoms before the age of 65) [3], [4]. In the UK alone, 40 000 people have young-onset cases of AD [5]. Alzheimer's Dementia (AD) is by far the most common form of dementia, constituting 62% of cases in the UK, and will be the main focus of this project [5]. It is characterised by the presence of the protein amyloid-beta (AB), the significance of which will be discussed later on in this section. Other major forms include vascular dementia, dementia with Lewy bodies, and a group of diseases that contribute to frontotemporal dementia. The boundaries between different forms of dementia are indistinct and mixed forms often coexist [3].

Dementia has high social and economic costs, both of which are likely to worsen for subsequent generations. It has been recognised as one of the major modern health challenges, a public health priorirty and an impending pandemic by the WHO [3]. At present, there are 7.7 million new cases of dementia every year worldwide [6]. In 2015, approximately 1.1% of the aggregated world GDP was spent on care and treatment, far exceeding the medical sector costs [7]. It is already the fifth leading cause of death worldwide [2] and the biggest killer in the United Kingdom [8]. In 2015, it was estimated that 850 000 individuals live with dementia in the UK, with a lifetime cost of £32,250 per person [5]. Furthermore, the ageing Baby Boomer generation will mean that dementia is likely to become an even more common, more costly disease over the next decade. It is projected that the number of people living with AD will rise by 55% by 2030 and 135.5 million people will struggle and ultimately die from AD by 2050 [6], [9].

AD leads to death of the brain's nerve cells, the neurons. The heathy human brain contains tens of billions of these electrical cells, processing and transmitting data to each other as chemical signals. They are one of two main cerebral cell types (glia), containing three basic parts: the cell body, numerous dendrites and the axon. When a neuron is instructed to fire, it generates an electrical signal that travels along the axon, releasing neurotransmitters across specialised contact points (synapses) to a neighbour's dendrite, either inhibiting or stimulating it. A fixed but highly dynamic web of 100 trillion interactions forms the basis of brain function [10]. AD injures and kills neurons throughout the brain, causing connections to break down and the network to fail. This results in cognitive impairment, brain atrophy and ultimately, death.

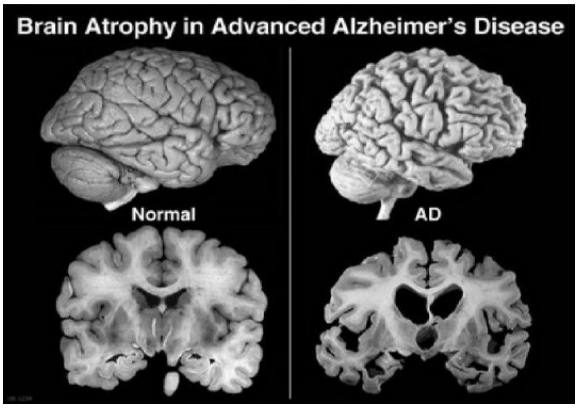

Figure 3.1: The shrinking of the brain in AD [11].

Amyloid-beta plaque build-up, another consequence of AD, is believed to be one of the causes of this neuronal death in what is known as the 'amyloid cascade hypothesis'. AB is the breakdown product of a larger protein amyloid precursor protein (APP), which normally plays an essential role in neural growth and repair [12]. Whilst low-level AB accumulation is common in ageing brains, small and dense AB plaque build-up has been found between neurons in all post-mortem examinations of AD patients. AB has been shown to be toxic to the nerve cells when it reaches these higher concentrations due to the harmful soluble AB oligomers [13]. Plaques are followed by the accumulation of neurofibrillary tangles within the neurons. These tangles are made of tau protein, the primary role of which is to maintain the stability of microtubules in the axons, which in turn transport nutrients and molecules from the cell body to the axon and dendrites. Tau proteins disintegrate into filaments that form tangles, harming this transport system and cutting off synaptic communication between neurons. AD induced atrophy occurs at three times the rate of a healthy ageing individual [10], as shown in Figure 3.1.

Despite the prevalence and the catastrophic consequences of AD, a cure remains to be found and, so

far, we are only capable of reducing the severity of its symptoms and delaying death by a few years. It is the only leading cause of death that we are currently unable to prevent or cure [14]. Whilst AD cost the UK health care system more than cancer and heart disease combined in 2012, it received six times less research funding than cancer [15]. Generalised as the cause of AD, the AB hypothesis has been the mainstream concept underlying AD research for over 20 years [16]. However, trial after trial have shown minimal benefits, leaving treatment of cardiovascular risk factors as the most efficient therapeutic treatment (discussed further in Section 3.2). This scientific deadlock shows that it is vital to pivot and explore other approaches to potential causes - for example, models of blood flow - due to the extreme cost of dementia to society.

3.2 The Role of Blood Flow

The constant supply of blood to the brain is vital for its proper function. Cerebral blood flow (CBF) regulates temperature, clears waste and carries oxygen and glucose for conversion to energy through metabolism. Although a healthy brain accounts only for around 2% of body weight, it accounts for up to 20% of the body's total energy usage [17], [18]. Between 75% and 80% of cerebral oxygen is consumed by the neurons, which inappropriately lack a nearby fuel reservoir to fulfil their dynamic and regionally specific energy requirements [17]. Therefore, this demand must be satisfied by blood flow. A short period of full ischaemia (full resriction of blood flow to tissues) will cause irretrievable brain damage, cell death and even a partial disruption to blood flow which can lead to chronic brain injury over a long period of time [19].

As explained in section 3.1, the impact of dementia is extreme cognitive decline. The following paragraphs will provide some evidence of how cerebrovascular pathology (CVP) and Alzheimer's dementia pathology (ADP) are related.

1. ADP and CVP frequently coexist [20], [21]. Post-mortem examinations of dementia patients show that ADP, accompanied by vascular lesions or parenchymal vascular disease (mixed dementia) is the most common form of dementia. In fact, only 24% of cases have pure ADP, whereas over 50% also have microinfarcts, microhaemorrhages, lacunar strokes or white matter lesions. Other microvasculature alterations are seen with ADP such as increased tortuosity, rarefaction, thickened basement membranes, presence of "string vessels" and increased atherosclerosis in intracranial vessels compared to age matched controls [22].
2. Epidemiological studies indicate a pathogenic role of vascular risk factors (VRF) in AD [23]. VRFs such as hypertension, cholesterol, smoking, etc. have been shown to increase cerebral amyloid

deposition through a combination of disrupted AB clearance and increased APP processing [24], [25], [26]. Controlling vascular risk factors, in some cases, delays the onset of AD and is currently the most effective therapeutic treatment available [27].

3. Several cerebrovascular disease risk genes have been identified which substantially increase the risk of AD. Apolipoprotein E (APOE) is a protein produced by astrocytes. Its $\varepsilon 4$ allele has been widely recognised as a shared risk gene, but recently, a greater subset of cardiovascular associated genes have been found to increase AD risk [28].
4. Hypoperfusion, a common pathology of many vascular diseases, has been shown to precede other AD pathologies. AB builds up 15 years pre symptoms, while biomarkers have shown reduced resting CBF up to 25 years before AD symptoms [29]. It is also the case that cerebral hypoperfusion is shown to accelerate the progression of AD [30] and attenuate hemodynamic responses to neural activity during this pre-symptomatic phase [31].
5. CVD presence has significant effects on the appearance and rate of cognitive decline [32]. CVD lowers the threshold at which AD manifests as cognitive decline, with some studies suggesting that there can be no cognitive impairment in AD without some level of CVD. Furthermore, cerebral hypoperfusion, a result of small-vessel CVD [33], has been shown to accelerate the progression of AD [30]. It is possible that this is a consequence of AD beginning to damage vessels before reaching the threshold of cognitive impairment, but further evidence implies a stronger synergistic relationship between the two. For example, it is the case that in lesions with minimal or no impact on cognition, one can get more severe dementia with the same degree AD pathology [34]. Furthermore, it is suggested that small-vessel CVD alters white matter pathology, integration and segregation. In turn, this impairs the recruitment of alternative cognitive networks or other cognitive strategies which might have mitigated ADP pathology [35]. For the UK, It has even been suggested that the recently reported reduction in the rate of increase in AD incidence may be due to improved cardiovascular heath [23].

The above evidence suggests CVD and AD may act independently through hypoxic-ischemic damage, or act synergistically, enhancing their respective impacts [36]. This appears to vary on a patient-by-patient basis, depending on factors such as cognitive reserve and genetic background, nature and the topology of CVD. In vivo, this is a very difficult relationship to unpick. Whilst improvement of biomarkers and better longitudinal studies may help, quantitative modelling should be done to help clarify the respective contributions and form of the relationship.

3.3 The Neurovascular Unit and Pericytes

The term neurovascular unit (NVU) was first coined at the 2001 Stroke Progress Review Group to highlight the special relationship between the brain's nerve cells and its vasculature, changing the (tacitly) held view of them as being mostly separate systems. While the exact cellular mechanisms remain somewhat unclear, the importance of the NVU is not. Recently, the view that neurodegenerative disease pathology, specifically AD, is separate and mechanistically unrelated from cerebrovascular disease (CVD) has been successfully challenged, with increasing evidence of NVU dysfunction being the missing link. The NVU is the intricate combination of reciprocally connected components: astrocytes, endothelial cells of the blood brain barrier (BBB), mural cells (contractile muscle cells) encircling the vessel wall, and neurones. The components are arranged in arterioles and capillaries as indicated in Figure 3.2.

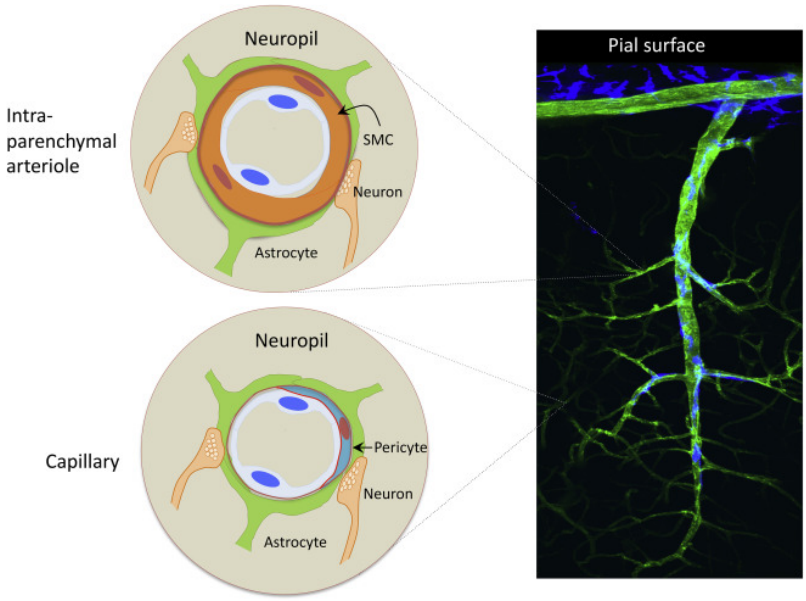

Figure 3.2: Diagram of NVU in cerebral arterioles and capillaries [37].

The primary function of the NVU is control of blood flow in the microvasculature (hyperaemia). It is also instrumental in brain development, the vessel cerebrovascular matrix (structural support and signal transduction), clearance of metabolic waste (notably AB) and is also the site of the BBB, amongst other functions [37]. Hyperemia is the process which regulates blood flow through small changes at a local level according to increases or decreases in neuronal demand by changing the vessel's intraluminal diameter. It is the combined response of hyperemia and autoregulation that determines the change in the vessel's intraluminal diameter to effect required CBF changes. Due to various scales and tissue needs, there is significant variation in the exact form of the NVU across the cerebrovascular tree.

The NVU's importance to CBF, especially in the microvasculature, implicates it in AD. The following paragraphs show various observed phenomena and papers that imply that there exists a relationship between NVU function and AD.

1. It has been suggested that oxidative stress induced by AB has pleiotropic effects on the NVU, damaging the endothelial and innate immune cells within the NVU [38].
2. BBB permeability increased in patients with prodormal AD, which refers to AD in the period between appearance of initial symptoms and the fully developed disease. This implies NVU dysfunction and a reduction in AB clearance [39].
3. Finally, neurovascular dysfunction has been linked to patients with cerebral amyloid angiopathy [40].

The focus of the model in this paper and a vital component of the NVU is the pericyte. This section will now define and explore its characteristics.

At the arteriole-capillary border, the mural cell is believed to transition from smooth muscle cell to pericyte. There is disagreement in the literature regarding this view, but essentially, this occurs due to a lack of effective biomarkers to distinguish between the pericytes and SMCs, and is in some cases, a definitional issue. The pericyte is suggested to exist in two distinct forms: longitudinal non-contractile and perpendicular contractile, which have a different way and process of wrapping around the capillary, shaping the pericyte like a claw [41].

The pericyte is interesting as the focus of a model for a variety of reasons:

1. The pericyte is specific to the capillary layer. Capillaries have small diameters and, as resistance to flow varies approximately inversely to the 4th power of the diameter due to Poiseuille's law, a large proportion of the vasculature resistance is supplied by the capillary layer. Therefore, small variations in capillary diameter are a practical method of controlling blood flow. Furthermore, most of the transfer of oxygen and glucose to the tissue take place over the capillary layer, the region where the pericyte is.
2. Pericytes have emerged as a novel therapeutic target for ischaemic heart disease, another flow related disease. The no-reflow phenomenon is the prolonged decrease of perfusion in tissue after ischemia even after upstream flow is restored. In some cases, perfusion has been halved in affected tissue. The pericyte has been identified as the culprit [42], pointing to its power for substantially altering blood flow and therefore, in our case, AD.

3. Pericytes have close contact with both neurons and astrocytes and exhibit contractile behaviour. This offers obvious potential pathways for them to be both effectors and sensors.
4. The CVD accompanying AD pathology has been found to be largely non-structural rather than structural damage, such as deformations in the vessel walls. Pericyte damage would class as structural damage so this is consistent [30].
5. Abnormal levels of soluble platelet-derived growth factor receptor B (Pdfr-B), associated with NVU coupling failure, has been measured in the cerebral spinal fluid in AD patients, which suggests pericyte degradation [39].
6. In living human brain tissue taken from biopsies, exogenous AB load has led to pericyte constriction [43]. Furthermore, pathways for this mechanism have been suggested; AB generates reactive oxidative species (ROS), mainly induced by NADPHs NOX2 and NOX4, triggering the release of endothelin-1 which contracts pericytes by acting on ET A receptors. Blocking NOX4 and ET A receptors stopped this process [44]. While most samples in this trial were ex vivo, contraction was also seen in venous and arterioles knock-in mouse models, suggesting a strong link between AB and pericytes.
7. Neurotransmitters have been shown to evoke pericyte-mediated vasoconstriction in situ [41].
8. Capillary constriction has been shown not to occur in areas free of pericytes [41].

This section has established that there is considerable evidence of the importance of pericytes and, more widely, NVUs, in AD. However, there is still some uncertainty on the topic. The research in the field is new and exciting.As pericyte and smooth muscle cells biomarkers and blood-oxygen-level-dependent imaging technology continue to improve, questions such as whether pericytes are able to both contract and dilate might finally be answered and the involved cellular mechanisms will become increasingly clear. Regardless, studying the pericytes' role in AD shows much promise.

3.4 Pericyte and Cerebral Blood Flow Modelling Research

Microvasculature models have often been treated separately to larger arterial tree models due to the difficulty in imaging vessels below 0.1 mm and the sheer number of vessels involved. This has meant that altogether different techniques need to be used [39]. Whilst it is the case that a few microvasculature models extend casts of small brain tissue volumes to the network, most models use construction algorithms that work using 'development rules' or attempt to satisfy known properties such as mean, standard

deviation, skewness etc. [45]. It should be noted, however that one criticism of such models is their high sensitivity to selection of blood haematocrit and pressure or flow boundary condition [46].

The methods used for solving blood flow are dependent on the network type, which means that they are often considered together in the literature. Coupled blood flow and network models generally fall under two categories; 1-D and 3-D. 3-D models include spatial information which is often derived from advanced imaging techniques, such as MRI. These models, especially models of human data, might be more credible clinically, but they are difficult and expensive to image. Thus, there are limited sample data available, making such models difficult to generalise from. It is also extremely difficult to image vessels of diameter below 0.1 mm, so 3-D models are seldom used for microvasculature modelling. On the other hand, 1-D models only use one spatial parameter: length. Often to work around the absent radial distance component, they use velocity integrated over the cross-sectional area to give a simplified representation of flow [47]. Although they are not always based on clinical data, simple bifurcation 1-D models without a complex flow pattern have been shown to be very accurate for a wide variety of uses, while also remaining less computationally expensive due to the reduced number of dimensions and assumptions involved in forming them. Therefore, a 1-D model will be used here for simplicity.

Historically, most 1-D models have consisted of a lumped model of the vasculature arteries, arterioles, capillaries and venules in series. For example, the Windkessel model combined all the microvasculature into a single resistance [48], or the vascular balloon model [49], which provided no opportunity for analysis of spatial features. A new network developed by Boas et al. (2008), called the vascular anatomical network (VAN), consists of studying thirteen small diameter microvasculature segments in parallel in a $0.006\,\mathrm{mm}^3$ scale invariant tissue volume, determined from measurable physical properties mainly from animal data, and a complementary flow model. The parallel nature of the model and its accounting for vessel resistance and oxygen delivery allows for better study of the dynamic response due to changes in segment properties. Payne (2018) has advanced the VAN by relaxing the constant length assumption and other assumptions through matching it to experimental data and updating the flow model accordingly. Parallel to the VAN, Reichold et al. (2009) developed the vascular graph model, based on the same principles and underlying equations. Its focus was, however, more geared towards applicability to realistic vascular networks through improved imaging techniques and extension to 3-D, although it lumps the capillary bed using up-scaling algorithms rather than keeping the capillary as discrete.

The updated VAN will be used for this project. While it was primarily developed for studying vascular tone response, it suits the purposes of this project due to its network precision and attached saturation and

blood pressure distributions. It also maintains a discrete capillary layer which allows for direct application of the pericyte response, which is the primary focus of this project. Furthermore, it allows the oxygen response to neuronal activity to be studied which is crucial for my analysis. Whilst it is true that the number of vessel generations used increases the computations required for each time step, thirteen generations will be manageable with the computational resources of this project. Neither the small tissue volume, nor the lack of imaging data will pose a problem to this project given that its aim is to investigate and loosely quantify the pericyte response rather than to gain clinical recognition where physiologically grounded and thorough models are more appropriate.

Literature modelling the pericytes' effect on diameter is lacking, so this paper will propose a novel model informed but not verified by experimental data. Various mechanisms have been suggested but there is no conclusive evidence on the pericyte response. Some literature suggests both a feed-back and feed-forward model of flow based on metabolic demand and neurovascular signalling pathways, showing the difficulties and uncertainties surrounding the topic [50], [51]. These responses are likely not to be mutually exclusive, therefore a simple model based on blood flow can be chosen, which incorporates elements of both models. Valuable data have been found on the pericyte response to ischaemia [52] which will illustrate the parameter values and characteristics of the control model. The extraction of these values will be covered in Section 4.1.

Further data has shed light on the proportion of pericytes that contract, not to flow, but to different signals. Of 30 pericytes studied, 27 constricted, beginning on average at 3.6 s and reaching maximum constriction at 12.6 s from electrical-stimulation-evoked constriction, with vessel constriction of 73% ± 5% for capillaries on straight parts. However, the proportion responding to neurotransmitters was much lower (25% to ATP in retina and 50% to nonadrenaline in cerebellum). Therefore, it will be worth exploring a responding proportion of pericytes within a large range [41].

Throughout this paper, it is important to stress that although models of blood flow and dementia exist, they are often based on a limited data set and so results should be taken with caution. More experimental data would certainly improve the models.

3.5 Conclusion

This literature review has provided the theoretical basis for the modelling of AD in terms of the role of pericytes. Despite the relative scarcity of experimental data, the existing studies were also helpful in allowing the comparison of this model to their findings.

4 Model Development

The following section presents the pre-existing approach chosen for modelling cerebral flow, the novel methods chosen for the unique modules and the numerical scheme used for this project. A modular structure was used, shown in Section 4.1, so that each unit could be examined individually and the result verified, which is done in section 5.1. The order of this section also shows the sequence of model development.

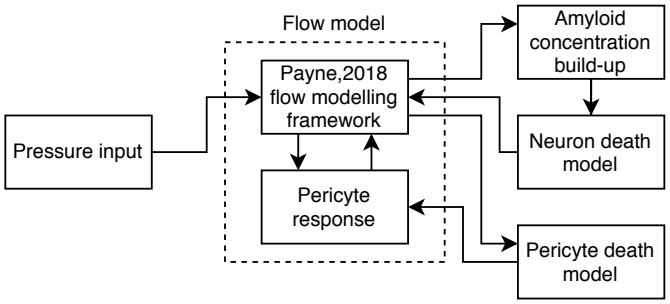

Figure 4.1: Block diagram illustrating structure of model.

To allow for reproduction of results, the values of constants can be found in Appendix A, alongside the baseline values from which the model is initialised and normalised. Normalised in this text will refer to scaling a parameter by its baseline value.

4.1 Network and Flow Model

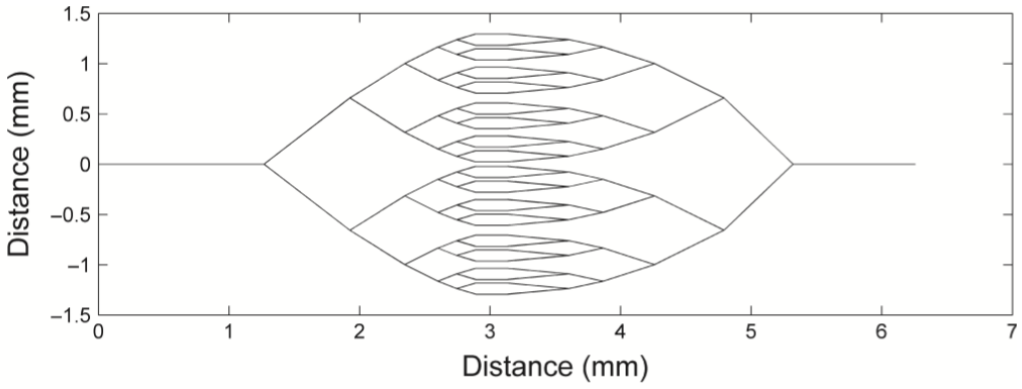

Figure 4.2: Diagram demonstrating the arrangement of the vessel network [1].

As laid out in Section 3.4, the basis of the network and flow model will be the updated VAN taken from Payne (2018). The most important features and governing equations alongside any deviations from this model will be stated. For further details and equations (omitted due to space constraints), please see

Payne (2018) [1].

The VAN is a 1-D bifurcating model consisting of a capillary layer linking six layers of arterioles and six layers of venules of decreasing and increasing diamaters respectively ranging from 7 to 32 µm. Payne (2018) has expanded upon this model, comparing and adjusting it against experimental data and forming methods to model previously ignored parameters. The number of assumptions is also reduced, making the network more general and therefore more applicable to the needs of this model. The parallel arrangement of the updated VAN is demonstrated in Figure 4.2, but it is worth noting that the only relevant spatial value is vessel length. The values are given in Appendix B.

The first difference in methodology from the Payne (2018) [1] paper is that the input for this project is arterial pressure (p_a), which is decreased in order to limit flow rate. The flow rate across the network can be found using a pressure-flow resistor analogy:

$$\Delta p_{network} = Q_{network}.R_{network} \tag{4.1}$$

where p is static pressure, Q is flow rate and R is resistance.

The resistance of the network is calculated using resistor methodology from individual vessel resistances. The resistance of a single vessel can be found using Poiseuille's law [53]:

$$R_{vessel} = \frac{128\mu L}{\pi D^4} \tag{4.2}$$

This project aims to include a pericyte health module based on a volume averaged partial pressure of oxygen in the tissues surrounding the vessels ($\hat{p}_t$). The VAN allows the tissue oxygenation levels to be considered on a vessel by vessel basis with the following governing equations derived from mass balance across both the tissues and blood vessels:

$$\alpha_t V_t \frac{\partial p_t}{\partial t} = \frac{2\pi KRL}{h}\left(\frac{1}{2}(p_{b,in} + p_{b,out}) - p_t\right) - MV_t \tag{4.3}$$

$$V_b \frac{1}{2}\left(\frac{\partial S_{in}}{\partial t} + \frac{\partial S_{out}}{\partial t}\right) + \frac{1}{2}\left(Q_{in} + Q_{out}\right)\left(S_{out} - S_{in}\right) = -\frac{2\pi KRL}{hc_{Hb}H}\left(\frac{1}{2}(p_{b,in} + p_{b,out}) - p_t\right) \tag{4.4}$$

where α_t is solubility of oxygen in brain tissue, V_t is tissue compartment volume around vessel, p_t is partial pressure of oxygen in the tissue compartment, t is time, K is oxygen permeability of vessel wall, R is radius of vessel, L is length of vessel , h is vessel wall thickness, p_b is partial pressure of oxygen in

the blood, M is rate of oxygen consumption in the tissue and in and out refer to the inlet and outlet of the vessel.

The inlet of each vessel segment corresponds to the outlet values of the previous segment, bar the first A1 segment which keeps constant pressure and saturation values at the inlet set by the model. A constant V_t has been assumed for each vessel. The Servinghaus equation was used to calculate p_b from S, which is updated by Equation 4.4, via a cubic solver [54]:

$$S = \left(23400(p_b^3 + 150p_b)^{-1} + 1\right)^{-1} \tag{4.5}$$

Another deviation from the updated VAN model is the change in the metabolism model. At small values of pressure and saturation, exponentially decreasing negative tissue pressure were seen, likely as a result of overshoot due to numerical error. A Hill equation style model with the constant metabolism' to attenuate its value at low p_t was used instead, which successfully prevented the instability:

$$M_{\text{hill}} = M_{\text{const}}\left(\frac{p_t}{p_t + \theta}\right) \tag{4.6}$$

The parameter θ is the hill constant. Figure 4.3 shows there is not considerable drop off from the constant metabolism value in the range of the baseline p_t values. The working metabolism only drops from the constant value by 20% as low as $p_t = 7.88$ mmHg.

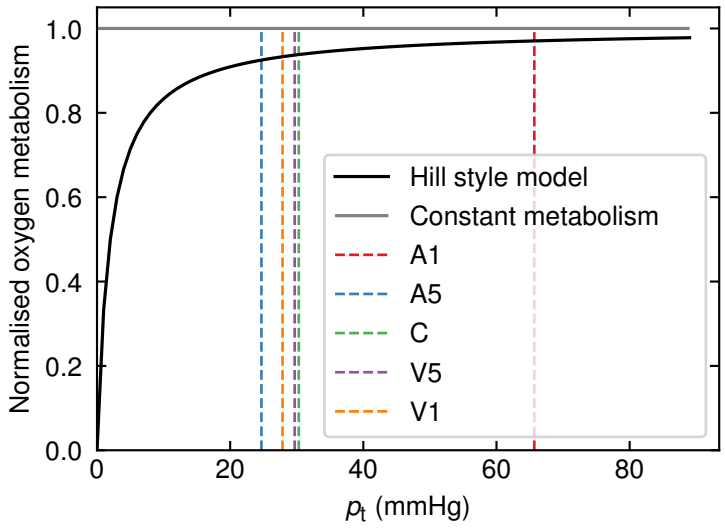

Figure 4.3: Illustration of the Hill style metabolism equation.

The steady state with no pressure drop will be referred to as the 'baseline conditions'. It is from these

conditions that the model is initialised. In the updated metabolism model, the baseline conditions differ from Payne's, but the values are sufficiently similar to make the change reasonable. Wherever sensible, variables have been divided by their baseline values and considered in terms of this normalised value. This serves to simplify units and allows easier comparison of the different result runs.

It is assumed that each vessel supplies oxygen to an independent volume of tissue, V_t , which is held constant to allow for changes in the oxygen concentration [1]. This volume is calculated for baseline conditions, balancing metabolic demand and oxygen supply using:

$$V_t = \frac{\overline{Q} c_{H,b} H \overline{\Delta S}}{\overline{M}} \tag{4.7}$$

4.2 Pericyte Response Model

Next, the pericyte response will be incorporated into the flow model. The various potential mechanisms for pericyte control mentioned in Section 3.4 are combined into a singular ODE controlling for capillary diameter, with an attached scaling function, based on flow rate. There is disagreement in the literature regarding the capillary as the primary microvasculature flow control effector. Here, we will assume that it is in fact the capillary that constricts. The exact location of the constriction will not strongly affect the response modes, so it is a satisfactory assumption in this project, regardless of whether in vivo the signal propagates to arterioles or even further upstream. Practically, all vessel diameters will remain constant bar the capillary diameter. A parameter ϕ will be used to represent the normalised capillary diameter. With our pressure drop initially reducing flow, ϕ will always be less than one and greater than zero. As some data suggest, not all pericytes respond to the flow stimulus, so we will use a factor α to represent the proportion that do contract.

The shape and constants for the pericyte response will primarily be taken from data in Hall et al. (2014) [52]. A least squares (LS) fit was performed on points taken from the effect of pericytes on capillary diameter in response to full ischaemia, shown in Figure 4.4, giving optimised values for response delay $\tau_d = 7.68\,s$, full ischaemia normalised diamter $\phi_{FI} = 0.153$ and pericte time constant $\tau_p = 2.29\,s^{-1}$. The following piecewise equation is a good approximation of the experimental data, giving a LS error of 9.10×10^{-3}:

$$\phi(t) = \begin{cases} 1 & \text{if } t <= \tau_d, \\ \phi_{FI} + \frac{1-\phi_{FI}}{\tau_p(t-\tau_d)+1} & \text{if } t > \tau_d. \end{cases} \tag{4.8}$$

The ϕ_{FI} is for full ischemia, so a parameter ϕ_{min} will be used to scale the response for partial flow

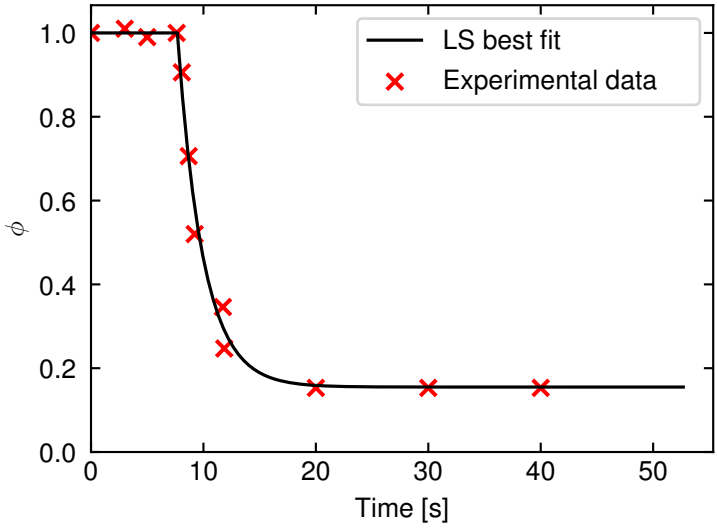

Figure 4.4: Fit to experimental data of the pericyte response in full ischaemia.

rates. ϕ_{min} is calculated as follows:

$$\phi_{min} = 1 - \alpha^{0.25}(1 - \phi_{FI})(1 - Q_{\text{norm}}) \tag{4.9}$$

This equation satisfies the boundary conditions of $\phi_{\text{min}} = \phi_{\text{FI}}$ at $Q_{\text{norm}} = 0$ and $\phi_{\text{min}} = 1$ at $Q_{\text{norm}} = 1$ when all pericytes are responding ($\alpha = 1$). The experimental response and scaling model were translated to a capillary diameter control model of the form:

$$\tau_{\text{p}} \frac{d\phi}{dt} = -\phi(t - \tau_{\text{d}}) + Q_{\text{norm}}(1 - \phi_{\text{min}}) + \phi_{\text{min}} \tag{4.10}$$

The parameter τ_p is the time constant of the pericyte response, ϕ is normalised vessel diameter, τ_d is delay of response for pericytes, Q_{norm} is normalised flow rate and ϕ_{min} is the pericyte response to partial flow rate scaling factor. This equation satisfies desired boundary conditions of stable diameter for baseline values ($Q_{\text{norm}} = 1$) and stable diameter at ϕ_{FI}.

The capillary vasoconstriction ties back into the model by decreasing the resistance and therefore decreasing flow rate. The resistance of a vessel has been shown (Equation 4.2) to vary inversely with D^4. Selecting a discrete number of capillaries to respond would limit α to certain discrete values and create issues in terms of selecting which capillaries react, as this would have a large effect on the resistance and take large amounts of time. Thus, the resistance of the capillary vessel was calculated using a weighted

average of the active and inactive resistance values in a lumped compartment approximation:

$$R_{\text{C,active}} = \frac{R_{\text{C,inactive}}}{\phi^4} \tag{4.11}$$

$$R_{\text{C}} = \alpha R_{\text{C,active}} + (1-\alpha) R_{\text{C,inactive}} \tag{4.12}$$

4.3 AB Accumulation Model

The accumulation of AB in tissue will be represented as a single concentration value for the entire network. It has been shown that reduced flow rate leads to a reduction in the clearance of AB. This accumulation is modelled using a first order ODE.

$$\tau_{\text{c}} \frac{dc}{dt} c = R - c(k + Q_{\text{norm}}) \tag{4.13}$$

The parameter τ_c is the time constant of AB accumulation, c is concentration of beta-amyloid. R and k are arbitrary values which can be set to bias the system towards sensitivity to flow rate or AB accumulation. The ODE is constructed so that when flow rate decreases, this triggers an increase in c. This increase in c then reduces the $\frac{dc}{dt}$ seen in Equation 4.13, allowing the concentration to reach a new steady state.

4.4 Pericyte and Neuron Health Models

A mass action kinetics style model will be used for the two remaining parts of the model: pericyte health and neuronal health. This involves classifying the state of the pericyte or neuron into three categories: alive, vulnerable or dead, as shown in Figures 4.5a and 4.5b. Then, rate constants determine the transformation from one constituent to another. Once a component is dead, it will not be given the chance to move back into the vulnerable or alive states. For initial conditions, it will be assumed that all neurons and pericytes are healthy.

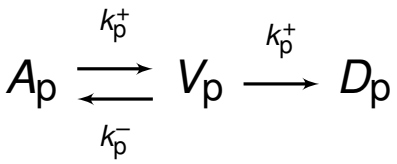

(a) Pericyte health model.

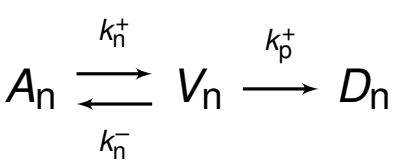

(b) Neuron health model.

Figure 4.5: The health models set up.

Here, A, V and D stand for alive, vulnerable and dead, and subscript p and subscript n denote pericytes and neurons respectively. The rate constants are given by k. Assuming our system is direct and has no intermediate steps, such that it is an elementary style reaction, the rate of reaction is equal to the product of the concentration of the species and its rate. The equations for change between compartments are:

$$\frac{dA}{dt} = -k^{+}.A + k^{-}.V \tag{4.14}$$

$$\frac{dV}{dt} = k^{+}.A - k^{-}.V - k^{+}.V \tag{4.15}$$

$$\frac{dD}{dt} = k^{-}.V \tag{4.16}$$

Using $A + V + D = 1$ unknown V can be eliminated from these equations to work purely in terms of A and D.

The rate constant equations will be based upon hyperbolic tangent functions. Hyperbolic tangent has been selected as it maps all inputs to an output between -1 and 1 and the sigmoidal shape attenuates the severity of the response at extreme values, maintaining a reasonable range of deterioration rate for the components. A general case in terms of x is as follows:

$$k(x) = \frac{k_{\text{const}}}{2}\left(1 \pm \tanh\left(\frac{x - x_{50}}{x_5}\right)\right) \tag{4.17}$$

The sign within the function is opposite for the forward (+) and backward (-) rate constant equation. It is set based upon whether you want an increases or decrease in the parameter controlling the system to elicit deterioration of the component. This is shown in Figure 4.6. The legend indicates the form of the forwards and backwards rate constants in the pericyte and neuron health models. The 50 and 5 values set the midpoint around which the response is measured and the sensitivity of deviation from this value respectively.

The rate constants for pericytes will be based upon the partial pressure of oxygen in the tissue as this is key in satisfying metabolic demand and maintaining health of the pericytes. We will define a volume averaged tissue oxygen partial pressure ($\hat{p}_{\text{t}}$) to represent the system, where N is the number of vessel segments:

$$\hat{p}_{\text{t}} = \frac{1}{\sum_{i=1}^{\text{N}} V_{\text{t,i}}} \sum_{i=1}^{\text{N}} p_{\text{t,i}} V_{\text{t,i}} \tag{4.18}$$

A smaller $\hat{p}_{\text{t}}$ implies that less oxygen is reaching the pericytes, therefore decreasing metabolism and

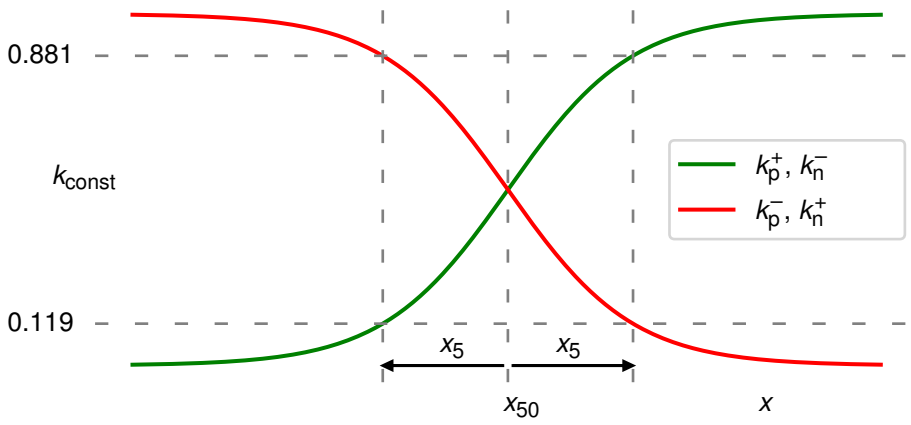

Figure 4.6: Illustration of the constant values set in the pericyte and neuron health models.

increasing the death rate of pericytes:

$$k_p^+(\hat{p}_t) = \overline{k}_p \frac{1}{2}\left(1 - \tanh\left(\frac{\hat{p}_t - \hat{p}_{t,50}}{\hat{p}_{t,5}}\right)\right) \tag{4.19}$$

$$k_p^-(\hat{p}_t) = \overline{k}_p \frac{1}{2}\left(1 + \tanh\left(\frac{\hat{p}_t - \hat{p}_{t,50}}{\hat{p}_{t,5}}\right)\right) \tag{4.20}$$

The toxic effect of AB on neuron health has been well-established. Therefore, the neuronal rate constant equations will be set based on AB concentration c:

$$k_n^+(c) = \overline{k}_n \frac{1}{2}\left(1 + \tanh\left(\frac{c - c_{50}}{c_5}\right)\right) \tag{4.21}$$

$$k_n^-(c) = \overline{k}_n \frac{1}{2}\left(1 - \tanh\left(\frac{c - c_{50}}{c_5}\right)\right) \tag{4.22}$$

Finally, the neuron and pericyte health equations are to be connected back into the flow model to create feedback loops. The pericyte control equation is thus adapted from Equation 4.10 to include the pericyte health:

$$\tau_p \frac{d\phi}{dt} = -\phi(t - \tau_d) + A_p\left[f(1 - \phi_{min}) + \phi_{min}\right] \tag{4.23}$$

As mentioned in the literature review, neurons make up approximately 80% of the energy demand of the brain tissue. Therefore, a decrease in neuron health would lead to a drop in tissue metabolism. A linear model is assumed here for simplicity:

$$M = A_n M_{hill} \tag{4.24}$$

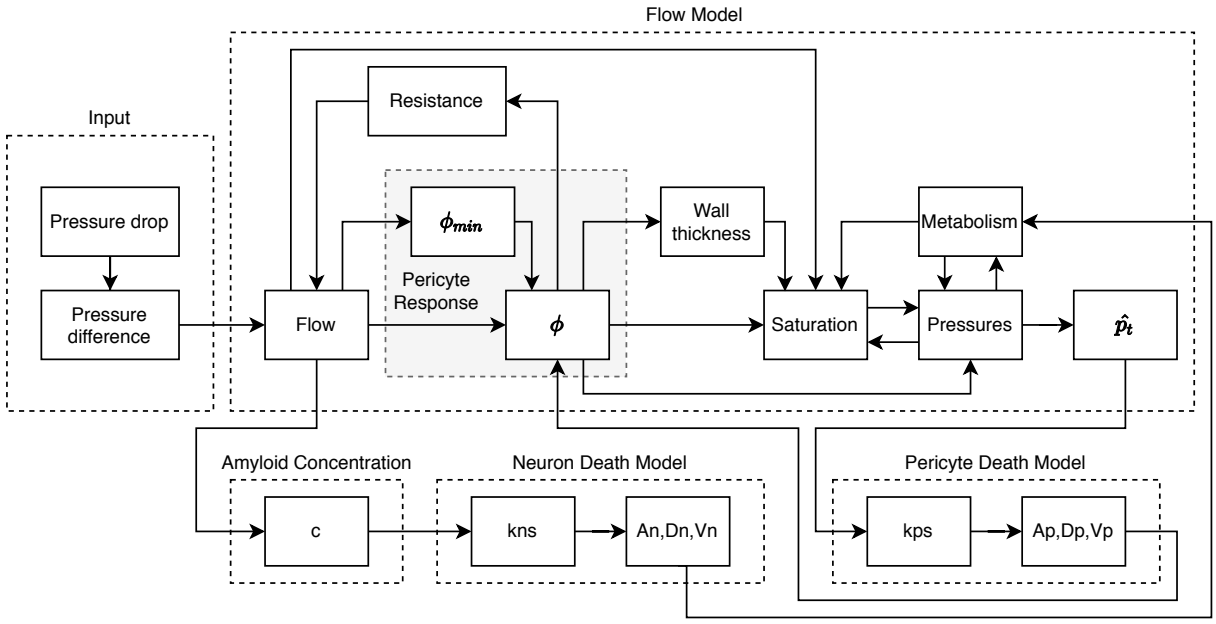

Figure 4.7: Full model block diagram of all parameters

where M_{hill} denotes the value of metabolism taken from the Hill equation.

This is a somewhat oversimplified way to analyse such a system, but it provides a pragmatic way of quantitatively measuring the survival of pericytes and neurons and how they can later affect certain physical processes.

4.5 Numerical Solver Details

As shown in Figure 4.7, this model has many interdependencies between different modules. Furthermore, there is one delayed differential equation and four ordinary differential equations to be solved for the overall system as well as a further three ODEs which are solved for each vessel (in total 39 times) for each time step. Therefore, while various numerical solvers are offered through MATLAB or Python, a bespoke solver was created to cope with the complex needs of the system.

Given that the model is an initial value problem, a Euler solver was first trialled during early testing of the flow model. When the smaller time constants of the pericyte and neuronal health models were added, the system became stiff in comparison to the short capillary response. This meant that a tiny time step was required for the forwards Euler solver. Instead, at this stage of the model development, a Runge-Kutta fourth order (RK4) solver was used as its global error of O(hˆ4) is considerably smaller than Euler's O(hˆ1). This significantly reduced the run time, given that the step size was able to be increased dramatically, even though the number of computations required per time step was approximately four

times greater. RK4 seemed to be a good middle-ground between ease of application and computational cost when compared with higher order models.

The standard RK4 equations have been extended to account for the multiple differential equations as follows, where h is the time step duration and n represents an arbitrary time step:

$$\frac{dy_i}{dt} = f(t, \mathbf{y}), \qquad \mathbf{y} = \begin{bmatrix} y_1 & y_2 & ... & y_k \end{bmatrix},$$

$$\mathbf{y}(t_0) = \mathbf{y}_0, \qquad \mathbf{a} = \begin{bmatrix} a_1 & a_2 & ... & a_k \end{bmatrix},$$

$$\mathbf{y}_{n+1} = \mathbf{y}_n + \frac{1}{6} h \left(\mathbf{a} + 2\mathbf{b} + 2\mathbf{c} + \mathbf{d}\right), \qquad \mathbf{b} = \begin{bmatrix} b_1 & b_2 & ... & b_k \end{bmatrix},$$

$$t_{n+1} = t_n + h, \qquad \mathbf{c} = \begin{bmatrix} c_1 & c_2 & ... & c_k \end{bmatrix},$$

$$a_i = f(t_n, \mathbf{y}_n), \qquad \mathbf{d} = \begin{bmatrix} d_1 & d_2 & ... & d_k \end{bmatrix},$$

$$b_i = f\left(t_n + \frac{h}{2}, \mathbf{y}_n + h\frac{\mathbf{a}}{2}\right),$$

$$c_i = f\left(t_n + \frac{h}{2}, \mathbf{y}_n + h\frac{\mathbf{c}}{2}\right),$$

$$d_i = f\left(t_n + h, \mathbf{y}_n + h\mathbf{d}\right).$$

When the primary values are updated for each stage of the solver, all dependent variables also have to be updated. The Python language was used to compile the model. For the full model, a simulation of 300 s took approximately 90 minutes to run, which was satisfactorily brief in order to explore various different input combinations.

4.6 Conclusion

This section has presented all the elements of the computational model which will produce the results of this project. These include the novel methods used to represent the pericyte response, AB accumulation and the the neuron and pericyte health models. It has also clarified where the flow model will deviate from that of the Payne (2018) VAN model. Finally, it has detailed the numerical system used.

5 Results

This section will present the main findings of the model. First, simulations involving only selected units of the model will be presented, in order to investigate they effect have on its stability and to ascertain whether the results returned are plausible. Then, results will be presented for the complete model as full-page figures of varying parameter values. This will involve changing the constants in order to see how they might affect the results. Finally, this analysis will be related to AD, which help determine which mechanisms are in line with AD research, which ones are not, and what can be what can be learnt from the model in terms of the pericytes effects.

The input to the model is an arterial pressure drop. The arterial pressure was initially maintained at baseline conditions for a brief period (often for 15s). This was done firstly to ensure that the model was behaving as expected and secondly to view the extent of the decay caused by the pericyte health model at baseline conditions. Then, a ramp was used to transition the arterial pressure to the desired final arterial pressure value, often taking 15s. This helps to limit the instability of the system, as opposed to using a pressure step change. The normalised pressure difference appears on relevant figures as a faint grey dashed line and will not be included in the legend of figures.

If a parameter value is not explicitly stated for a given simulation, it can be assumed that it is the 'default' value, which can be found in Appendix C. Also, Appendices B and A display the assumed network properties and constants. Finally, to view the interactions between different parameters, please reference the block diagram in Figure 4.7.

5.1 Individual Unit Results

This section aims to ensure that each unit behaves in a plausible way and to gain insight into how each unit effects the flow model's response. This will allow for greater understanding and analysis of the mechanisms in the full model results. In each subsection, the relevant parameters to the stage of the model being investigated will be shown in a block diagram. This will be built upon progressively towards the full model with consistent block positioning to allow for easy comparison between subsections.

5.1.1 Base Flow Model Results

This section will show the results of the flow model outlined in Section 4.1. This constitutes the basic response of the full model and it is from these results that the effects of the various processes are

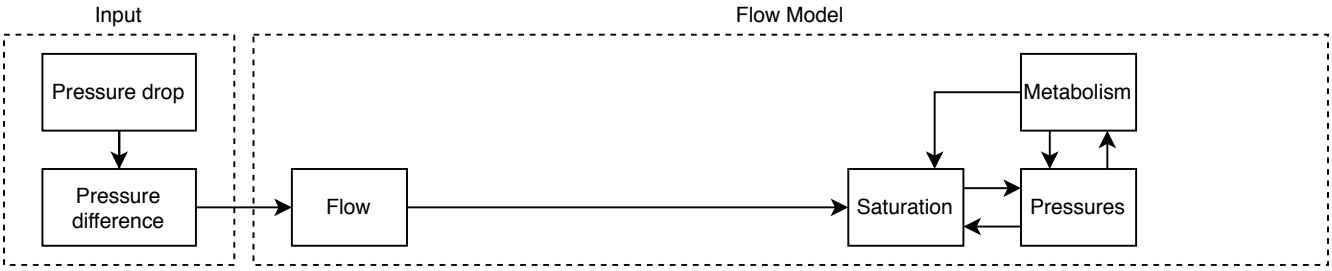

Figure 5.1: Block diagram illustrating the parameters in the flow model.

measured. The active parameters for this simulation are shown in 5.1. The results are shown in Figure 5.5.

Figure 5.5A shows that the flow rate is directly proportional to the pressure drop, as expected. This is due to the diameter of the capillary bed remaining constant. Therefore, there is no change in the resistance of the network. Figure 5.5B shows p_t for a selection of the vessels to indicate the behaviour of the entire vessel distribution. An exponential first order style dynamic response is seen during the pressure difference transition. The p_t response takes marginally longer to arrive at steady state than the flow rate response. This is caused by the variation of the vessel specific metabolism due to the Hill-style equation. This effect is most pronounced for larger diameter arteries. Otherwise, the p_t distribution mirrors the flow rate distribution.

5.1.2 Pericyte Response Results

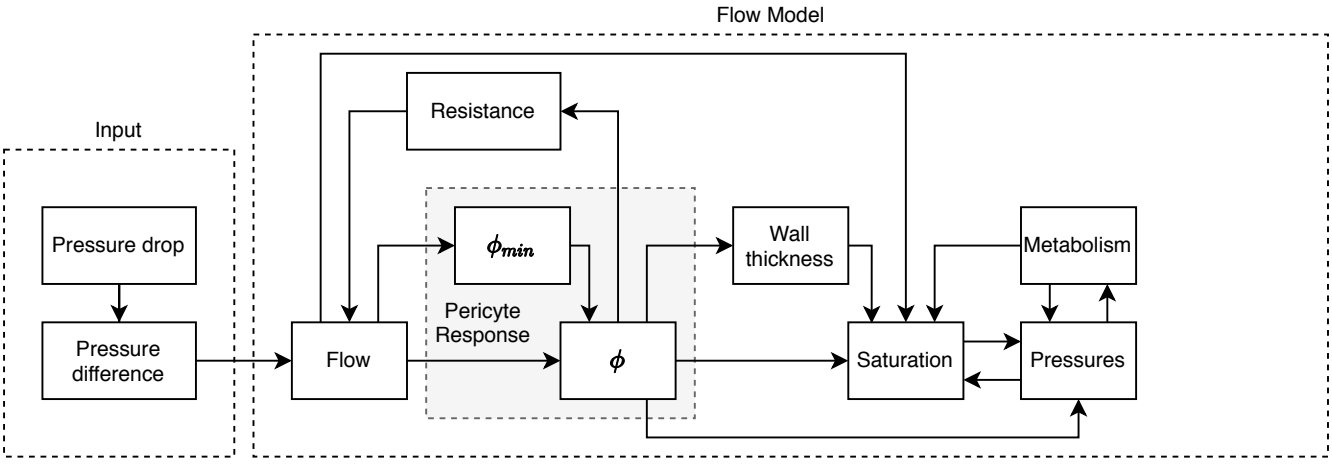

Figure 5.2: Block diagram illustrating the parameters in the pericyte response model.

This section will investigate the effect of including the pericyte response model on the basic flow model. The results are shown in Figure 5.6. Figure 5.6A shows that the flow rate steady state is slightly lower

than for the base flow model. This is due to the change in the capillary bed diameter marginally increasing resistance, as shown in Figure 5.6B. This mechanism is controlled by a small feedback loop initiated by the pressure drop, which is illustrated in Figure 5.2. The capillary is prompted to constrict, increasing resistance of the network and in turn further decreasing flow rate and capillary diamater. The effect this has on the resistance is shown in Figure 5.6D. The response of ϕ_{min}, shown in Figure 5.6C, limits the loop's growth.

In order to validate the model, the expected steady state values can be found and compared against the steady state values of this simulation. The expected steady state is found by setting the time varying derivatives of equations 4.3, 4.4 and 4.10 to zero:

$$0 = \frac{2\pi KRL}{h}\left(\frac{1}{2}(p_{\text{in}} + p_{\text{out}}) - p_{\text{t}}\right) - MV_{\text{t}} \tag{5.1}$$

$$\frac{1}{2}\left(Q_{\text{in}} + Q_{\text{out}}\right)\left(S_{\text{out}} - S_{\text{in}}\right) = -\frac{2\pi KRL}{hc_{\text{Hb}}H}\left(\frac{1}{2}(p_{\text{in}} + p_{\text{out}}) - p_{\text{t}}\right) \tag{5.2}$$

$$0 = -\phi + Q_{\text{norm}}(1 - \phi_{\text{min}}) + \phi_{\text{min}} \tag{5.3}$$

These equations are solved for using an attractive fixed point numerical system. The values found were within a small tolerance of the simulation's steady state values, validating the results of the simulation. For example, the steady state values predicted by the iterative solver for Q_{norm} and ϕ are plotted as a horizontal lines in Figures 5.6A and 5.6B.

5.1.3 AB Accumulation Model Results

The next elements to be included in the model and simulated are the AB accumulation and $\hat{p}_{\text{t}}$. These two parameters are related as they control neuron and pericyte health models respectively. The results for the flow model and the pericyte response have been re-run to include these metrics and are shown in Figure 5.7. The block diagram in Figure 5.3 shows that neither will affect the flow model, so figures for flow rate will not be shown. It should be noted that the inclusion of the AB accumulation model has dramatically increased the number of iterations required in the simulations.

Figures 5.7A and 5.7C highlight the similarity in the accumulation of AB for both the flow model and the perciyte response, implying that without the later included health models, the pericyte response does little to affect AD. As discussed in Section 4.3, c depends entirely on flow rate. As flow rate is similar for both simulations, we get similar c distributions. $\hat{p}_{\text{t}}$ is a linear summation of the p_{t} values, hence Figures

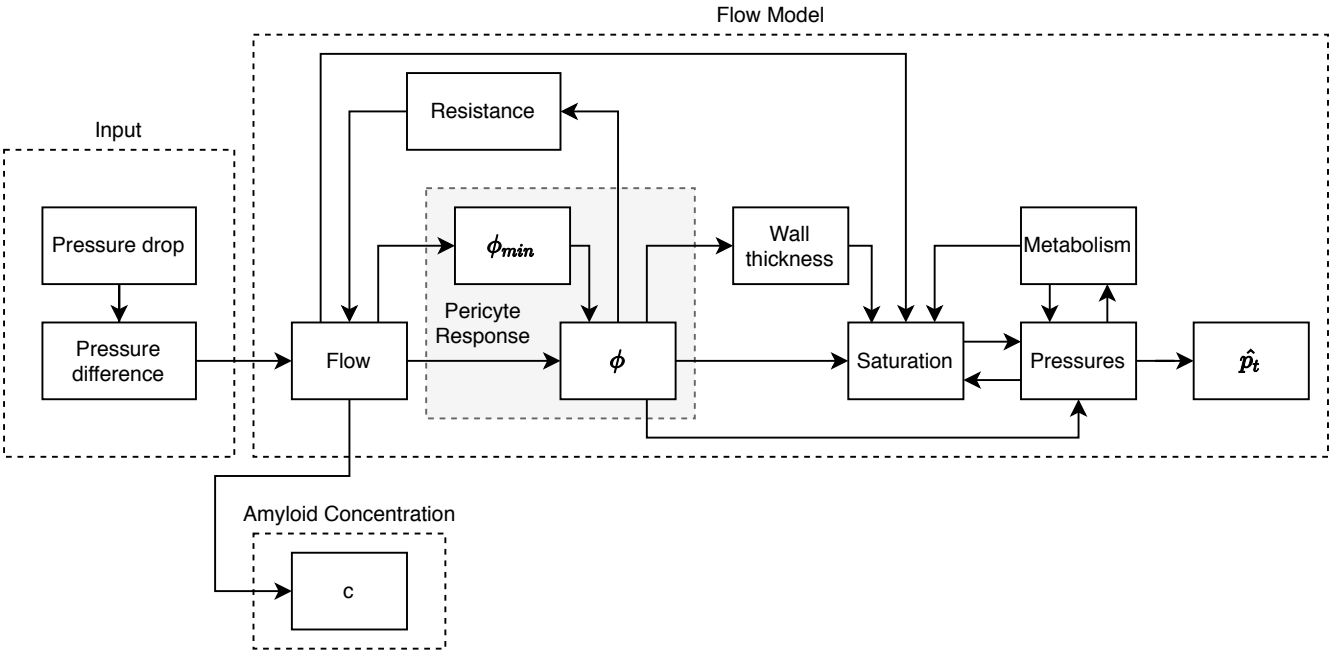

Figure 5.3: Block diagram illustrating the parameter relationship for the flow model with health metrics.

5.7B and 5.7D display a similar exponential first order-style response for $\hat{p}_t$ during the pressure difference transition.

5.1.4 Pericyte and Neuron Health Model Results

Finally, the pericyte and neuronal health models will be included in the simulation, which will complete the full model shown in Figure 5.4. Due to their similar form, both health models results will be examined and then compared in this section. To examine the pericyte health model, the rate constants of the neuronal health model are set to zero and vice versa for analysing the neuronal health model. The results for inclusion of each health model can be seen in Figures 5.8 and 5.9.

Before discussing the flow rate results, it is important to understand the ϕ response. Figure 5.9B shows that the ϕ response of the neuron health model simulation is similar to the responses shown earlier in this section, for example in Figure 5.6B. Therefore, the flow rate and *c* responses shown in in Figures 5.9A and 5.9D also remain similar to the earlier results due to their reliance on resistance and ϕ.

However, the pericyte health model simulation ϕ response differs from the flow model response. Figures 5.8B shows a continued steady decrease in ϕ past the steady state value of the neuron health model simulation. This is due to the effect of A_p in the pericyte response in Equation 4.23. Its inclusion means that death of the pericytes further constricts the diameter of the capillary bed beyond the normal limiting ϕ_{min} value. The linear decrease seen in ϕ in Figure 5.8B corresponds to the linear change in A_p

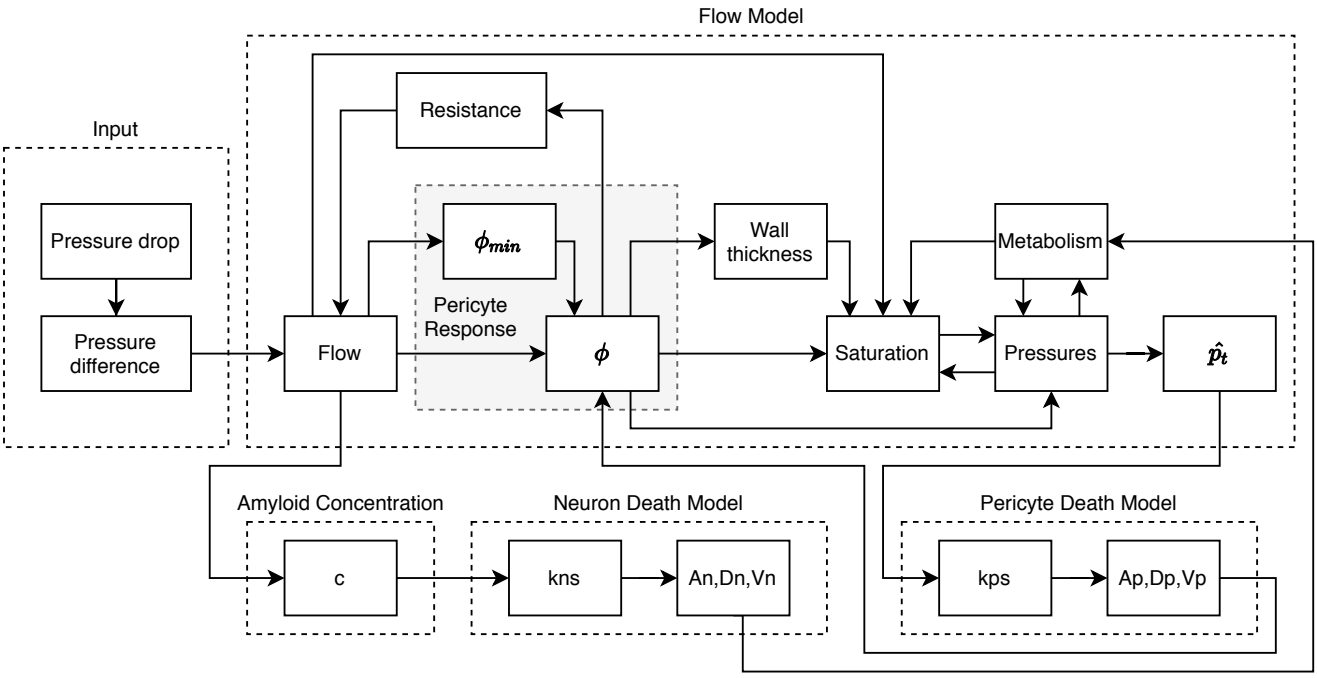

Figure 5.4: Block diagram illustrating the parameter relationships for the full model.

for this simulation, shown in 5.8F. This increases the resistance of the network. The flow rate shown in Figure 5.8A decays in response to this increasing resistance. This non-linear mechanism will be described in more detail in the full model default values simulation discussion in Section 5.2.1, where the effect of the mechanism is more prominent. The flow rate decay causes c to increase, as shown in Figure 5.8D. Furthermore, the p_t values in Figure 5.8E decay causing $\hat{p}_t$ in Figure 5.8C to decay as well.

Figure 5.9E shows the effect of including the neuron health model for the p_t response. The p_t values actually rise in the vessels, causing the $\hat{p}_t$ in Figure 5.9C to increase as well. This is caused by the reduction in A_n, shown in 5.9F. As neurons die, the metabolism of the tissue decreases via Equation 4.24. Therefore, it is possible for oxygen levels to build in the tissue under these conditions.

The observations of the isolated responses described in this section will allow the consideration of the trends of the full model in Section 5.2. It appears that pericyte health has more bearing on the response of the system than neuronal health due to its ability to affect both flow rate and the pressures of the system. The combined full model response involving both health systems will be explored in the next section.

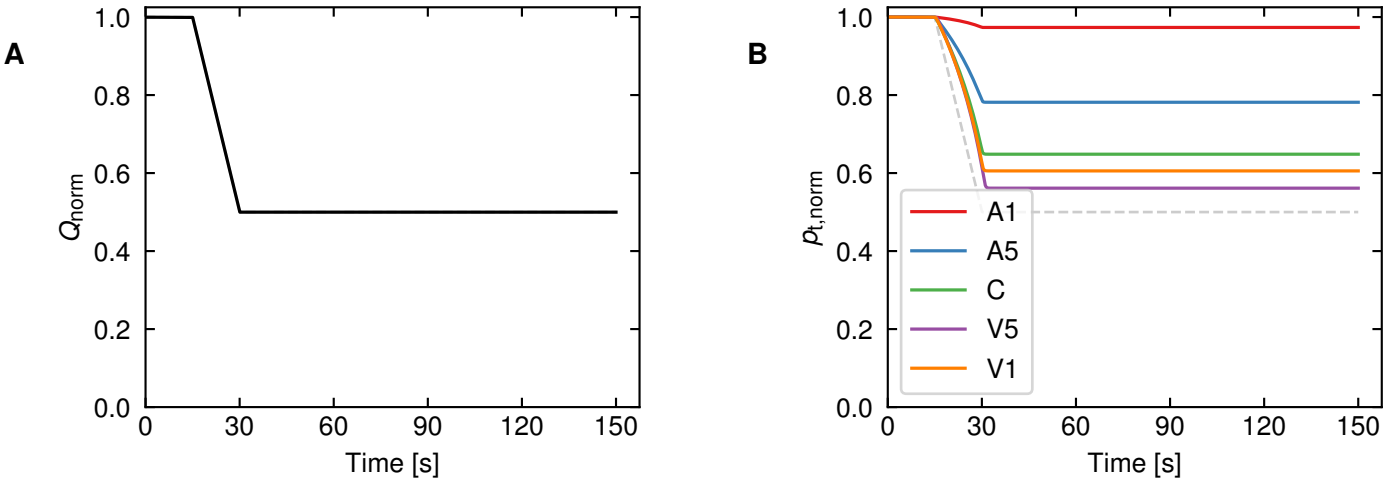

Figure 5.5: Base flow model results.
A: normalised flow rate response; **B**: the distribution of the normalised partial tissue pressure of oxygen surrounding a selection of vessels.

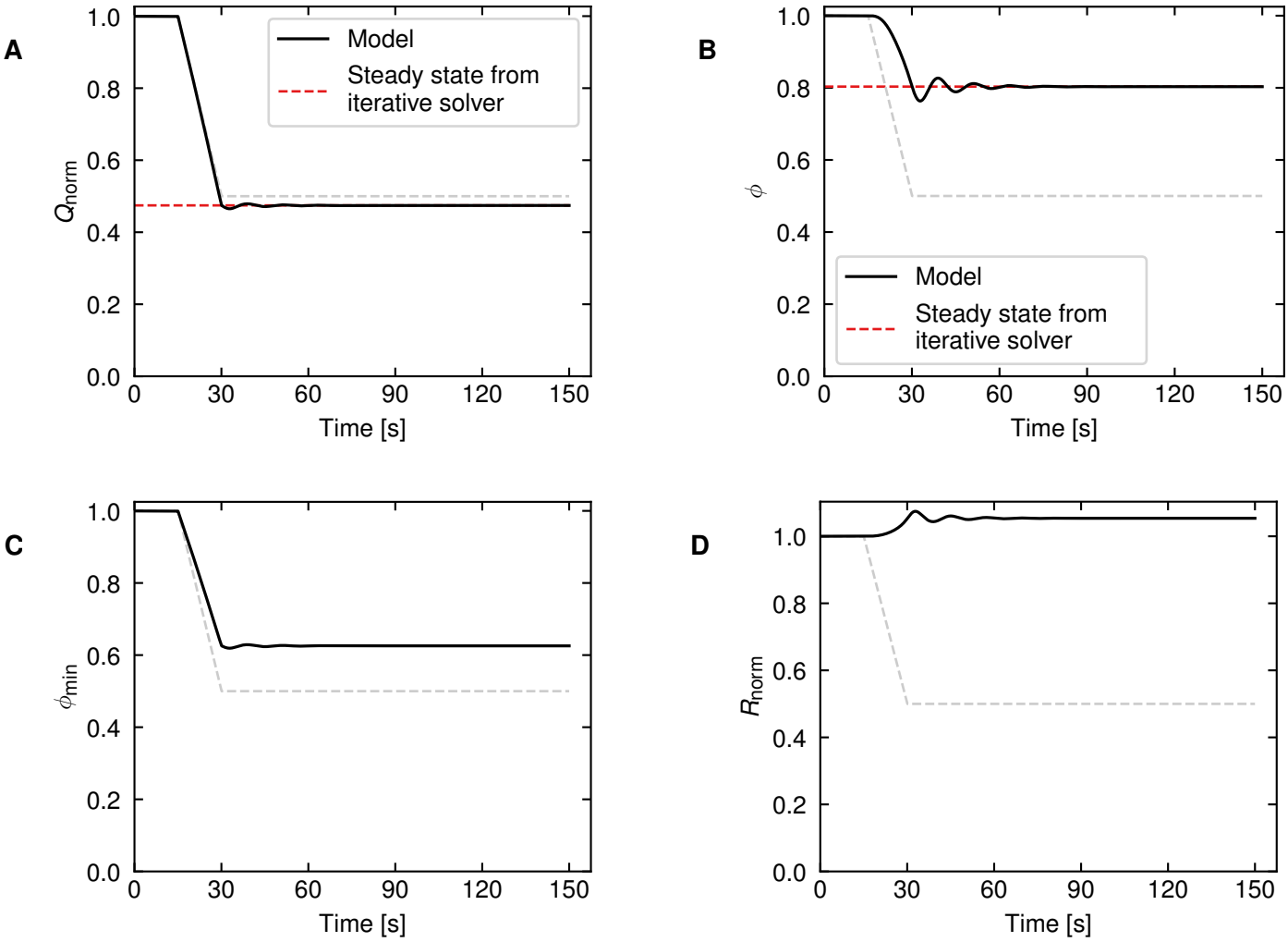

Figure 5.6: Pericyte response results.
A: normalised flow rate response; **B**: normalised capillary bed diameter response; **C**: ϕ_{min} scaling factor; **D**: normalised total resistance of the network.

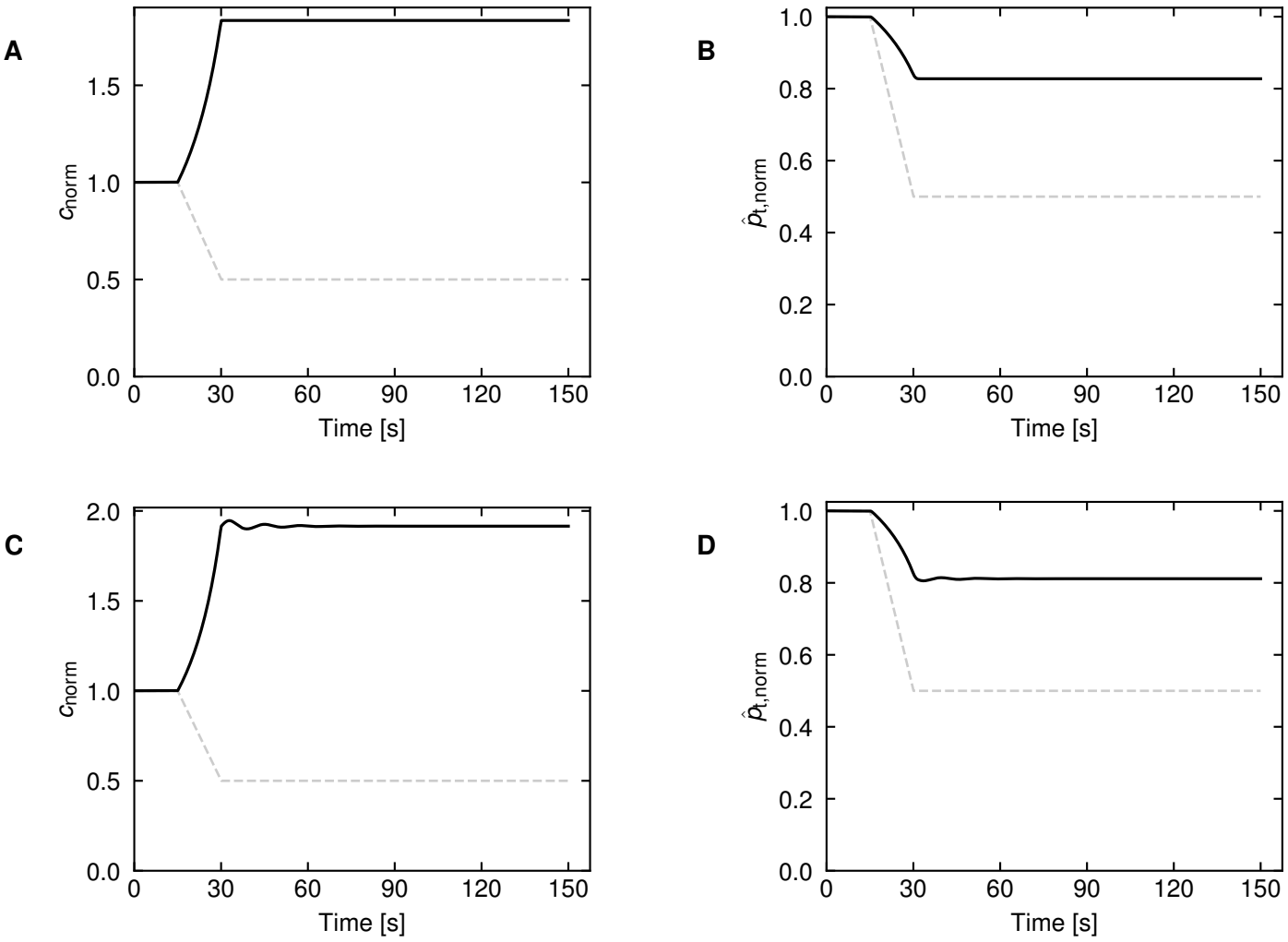

Figure 5.7: Health metrics.
A & **B**: AB concentration and $\hat{p}_{t,norm}$ plots for the flow model; **C** & **D**: AB concentration and $\hat{p}_{t,norm}$ plots for the pericyte response model.

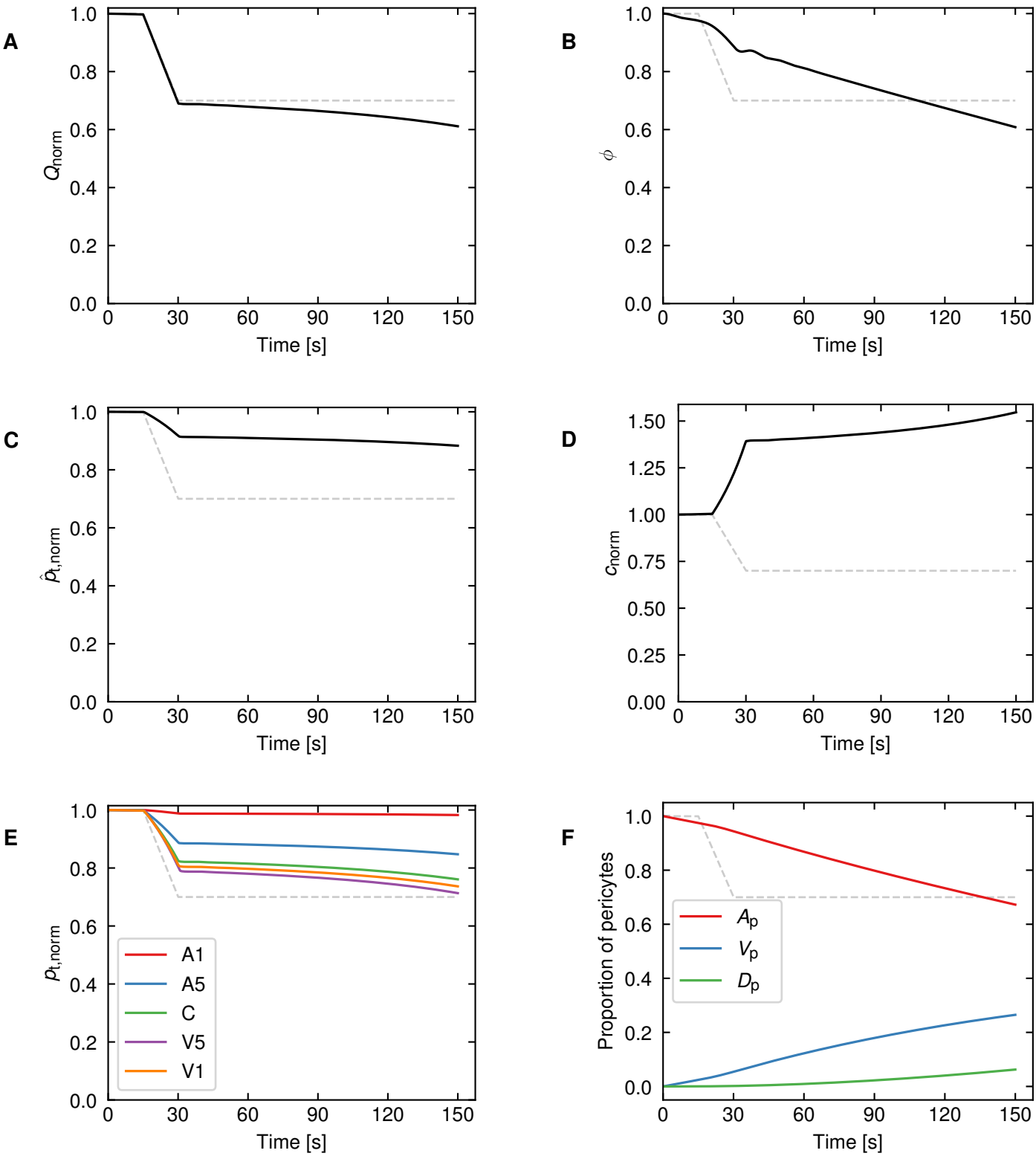

Figure 5.8: Pericyte health model results.
A: normalised flow rate response; **B**: ϕ response; **C**: $\hat{p}_t$ response; **D**: normalised AB concentration response; **E**: normalised vessel p_t response; **F**: pericyte health model states.

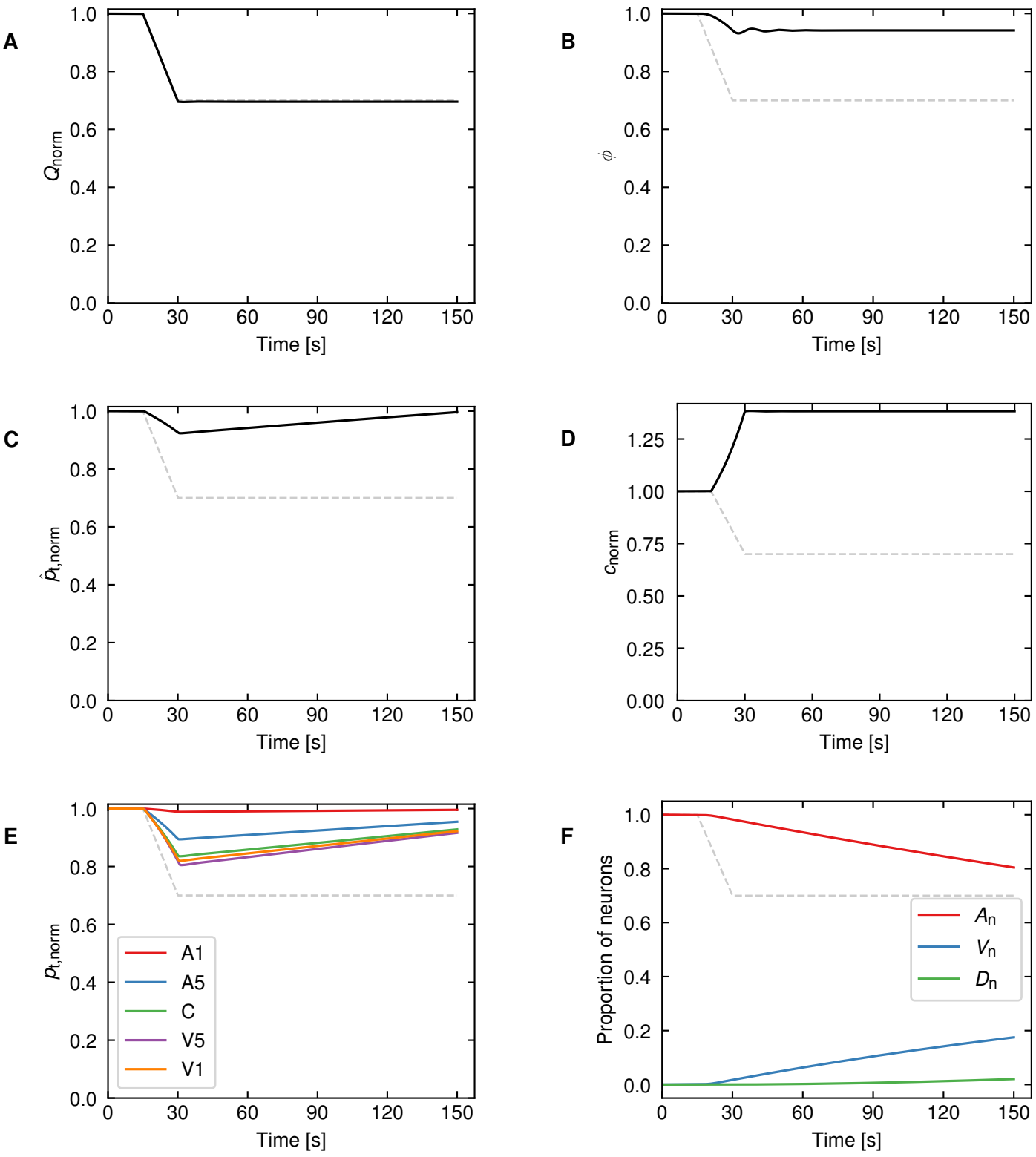

Figure 5.9: Neuron health model results.
A: normalised flow rate response; **B**: ϕ response; **C**: $\hat{p}_t$ response; **D**: normalised AB concentration response; **E**: normalised vessel p_t response; **F**: neuron health model states.

5.2 Full Model Results

This section will involve the analysis of the full model response. The results of the previous section on the individual units of the system will be useful for understanding the mechanisms driving these results. An attempt will be made to separate the effect of individual parameter values on the death of neurons, flow rate and the accumulation of AB. Over 150 simulations lasting between 300 s and 2400 s of various parameter values were completed as part of this study. A selection of them will be presented over the first part and the discussion of their results will follow. First, a control will be presented with the default values, which was selected due to its shape typical of the model. Then, the effects that changes in individual values have on the results is discussed. Finally, characteristic responses for the full model are covered. The figure relevant to a discussion is referenced in the section title.

5.2.1 Default Run Discussion (Figure 5.11)

As stated in the introduction to this section, this run has been chosen for its typical response. A similar deterioration in neuron and pericyte health models is seen and the time taken for the flow rate to tend to zero is typical. The values used in this simulation will be referred to as the default values; they can be found in Appendix C. This discussion will focus on the different regimes of flow rate response and the dominant processes in these regimes, as they form the basis of the analysis of the following simulations in this chapter.

The flow rate response, shown in Figure 5.11A, has the three main parts: the initial approximately constant flow rate between 0 s to 15 s, the approximately linear drop in flow rate between 15 s to 30 s and the exponentially decaying flow rate drop from 30 s until $\approx$ 550 s, where it tends to zero. To understand the observed response, it is important to understand how resistance, linking pressure drop to flow rate, is calculated for the network.

The resistance of the network can be seen as the sum of two parts: the constant resistance of the constant diameter vessel segments and the varying resistance of the dynamic diameter capillary segment. The project assumes the resistance of the capillary segment is calculated via a weighted average, a combination of the non-contractile constant resistance proportion and the flow-responsive contractile varying resistance proportion (see Equation 4.12). A simplified version is given here below, where all constant terms are represented as R_{constant} and $\overline{R_C}$ is the capillary vessel baseline resistance:

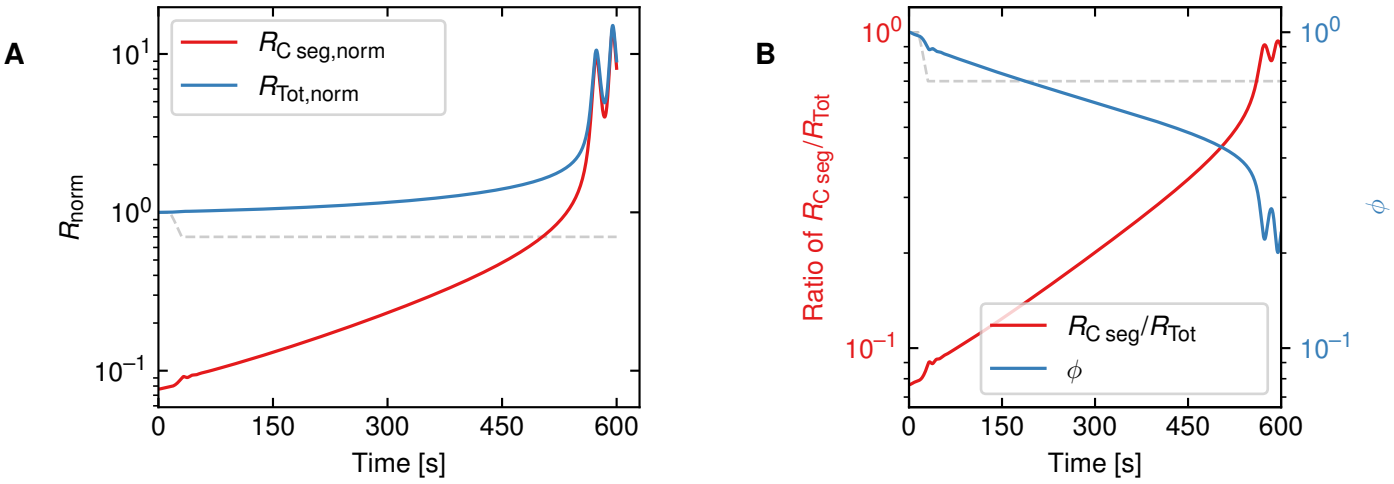

Figure 5.10: Resistance contribution of the capillary layer for the default values simulation. **A**: Comparing the total network and capillary segment resistance normalised by the baseline total network resistance; **B**: Highlighting the correlation between the proportion of the total resistance contributed by the capitally segment and the diameter of the capillary bed.

$$R_{tot} = R_{const} + \frac{\alpha \overline{R_C}}{2^6 \phi^4} \tag{5.4}$$

$$\frac{dR_{tot}}{d\phi} = -\frac{\overline{R_C}}{2^4 \phi^5} \tag{5.5}$$

The differential means that, for the small negative changes in ϕ that arise in this project, the increase in R_{tot} is greater for small values of ϕ.

The other part to consider is the relative size of the resistance terms. Initially, at $\phi = 1$, the capillary segment contributes only 7.66% of the total baseline network resistance. Figure 5.10A shows how for the default values simulation, the capillary segment contribution increases to the point where it converges with the total resistance of the network. Figure 5.10B shows the correlation between ϕ and the relative contribution of the capillary segment to the total resistance.

Referring back to Figure 5.11A, ϕ remains above 0.96 (shown in 5.11B) during the first 15s of baseline pressure, so there is little change in resistance. Thus, the flow rate remains close to baseline conditions. During the pressure drop phase, flow rate drops marginally further than the pressure difference, due to increased resistance. However, ϕ still remains high (above 0.9), so network resistance changes only by a small fraction. The third section of exponential decay is where this non-linear ϕ and resistance relationship begins to dominate. ϕ drops steadily from 0.9 at $t = 30$ s to 0.4 at $t \approx 550$ s which leads to an exponential

decrease in the flow rate, due to the exponentially increasing resistance.

The ϕ shown in Figure 5.11B decreases linearly, in a manner very similar to the 5.1.4 results. Therefore, it will not be discussed again.

Figure 5.11C shows the AB concentration response. For the first 30 s, c mirrors the flow. After 30 s, c builds at a relatively lower speed than flow rate decreases. Once flow rate begins to tend to zero, a spike is observed in the concentration of AB, as would be expected.

The behaviour of $\hat{p}_t$ in Figure 5.11D is steady until flow tends to zero. The steady nature is actually the combination of two opposite effects. While the flow decrease tends to reduce $\hat{p}_t$, the neuronal death is counteracting this by reducing metabolism and therefore increasing $\hat{p}_t$.

Figure 5.11E shows an approximately 50% reduction in A_p and 20% rise in D_p across the course of the simulation. Figure 5.11F shows a similar final value for A_n, but with a much lower final portion of D_n. This is due to the curved shapes for A_p and D_p. As the pericytes changed more rapidly, the alive and vulnerable proportion has been on average higher over the simulation. As the rate of change in state depends on the concentration of that state, more pericytes have reached the dead state. This highlights the importance of the distribution shape on the final values.

5.2.2 Individual Parameter Effects

Next, the effect of the most important input parameters on the model will be evaluated: the pressure difference input, the delay of the pericyte response and the proportion of pericytes that respond. These three parameters collectively have a large effect on the stability of the model, which is also briefly discussed. The parameter effects are referenced against the default values response (Figure 5.11).

Pressure drop effect (Figure 5.12)

The effects of dramatically increasing and decreasing the pressure drop are shown in Figure 5.12. The result that higher pressure drop simulations tend to zero flow rate faster is expected. This confirms the importance of the initial pressure drop on the time taken for the system to decay. Additionally, the shape of the flow rate after pressure drop of these two responses is similar, while diverging at greater time ranges.

Delay effect (Figure 5.13)

Extracted from experimental data, the delay of the pericyte response, τ_d is 7.68 s, as outlined in Section 4.2. However, using this value alongside the other default system values leads to an unstable

response. It has been found that increasing α to 0.5 allows the desired delay of 7.62 s to be simulated. This is why a delay of 2.5 s is used as the default value.

From the results in Figure 5.13, one can see that the delay value has little effect on the results of the simulation. Conversely, it does have a great effect on the stability of the model, with no simulations of delay greater than 12s being possible under any input conditions. This could be due to it being a relatively small time constant compared to other time constants in the system (i.e. pericyte and neuronal health systems). However, decreasing the time step duration does not significantly increase the possible values of α and τ_{d} that are stable.

Proportion of pericytes responding effect (Figure 5.14)

Beyond the stabilising effect of α described above for the delay value, α has substantial effects on the model results. A zero α value would give an identical response to the model without the pericyte response. Figures 5.14A and 5.14B show that for a high α value, the flow rate and capillary diameter decay is rapid.

5.2.3 Characteristic Responses Discussion

This next section will present simulations that offer points of discussion for the model. All results are referenced against the default values response (Figure 5.11).

Slow response discussion (Figure 5.15)

The death of pericytes and neurons would happen over the order of years in an AD patient, so an important test of this system is increasing the time constants from the order of minutes (which is the range often used for simulations in this project). Figure 5.15A shows that halving the two rate constants has quadrupled the time taken for the system to tend to no flow compared to the default values simulation. It would be reasonable to assume that further decreasing of the constants would lead to slower flow responses. Unfortunately, simulations of this duration are outside the scope of this project, but in the future may lead to more clinically relevant results.

Figures 5.15E and 5.15F show that the proportion of dead pericytes and neurons for this longer duration run are much higher at the point of no flow being reached. Figures 5.15A, 5.15B, 5.15C and 5.15D show that the shapes of the other variable response are similar to the default model.

Accelerated response discussion (Figure 5.16)

An aspect of the model set-up that proved particularly important was setting the 50 and 5 values for the

hyperbolic tangent rate equations. This is because they elicit great variance in response. In this response, the $\hat{p}_{t,5}$ was set an order of magnitude lower than for the default values simulation. The constants in the pericyte health model were set as follows:

$$\hat{p}_{t,50} = \hat{p}_{t,baseline} \tag{5.6}$$

$$\hat{p}_{t,5} = 0.1.\hat{p}_{t,baseline} \tag{5.7}$$

Initially, the rate of pericytes moving towards the vulnerable and dead states was half of the maximum rate. The subsequent drop in $\hat{p}_t$ seen in Figure 5.16D was relatively large compared to the small $\hat{p}_{t,5}$ set for this simulation, effectively maximising the rate of death of pericytes. This caused the ϕ value, shown in Figure 5.16B, to decrease rapidly. This was then followed by a rapid and characteristic decrease in flow rate, seen in Figure 5.16A.

Conversely, setting $\hat{p}_{t,50}$ too low would mean that no pericyte death would occur and the results would be effectively the same as the case with no pericyte health model included. These two cases highlight that the model is extremely sensitive to the values chosen for $\hat{p}_{t,50}$ and $\hat{p}_{t,5}$. Experimentation found that setting a large $\hat{p}_{t,5}$ prevented the rapid death of the simulation and allowed various combinations of variables to be explored.

Second equilibrium response (Figure 5.17)

Another interesting phenomenon surrounds neuron death, as exhibited in Figure 5.17. Initial rapid neuron death appears to stabilise pericyte death and therefore the flow rate. This is in stark contrast to rapid pericyte death, which causes rapid decay and death of the system.

Neuron death initially outpaces pericyte death in this response, shown in the comparison between Figures 5.17E and 5.17F. Due to the A_n linearly scaling in the metabolism calculation, this causes the metabolism of the tissue to decrease rapidly, leading to tissue pressure values significantly above their baseline values, as shown in Figure 5.17D. As the pericyte health is controlled by $\hat{p}_t$, not only does this increase cause pericyte degradation to slow, but vulnerable pericytes begin to move back into the alive state. A second plateau appears in the flow rate diagram (Figures 5.17A) due to this stabilisation of A_n.

This result implies that when neuron death significantly outpaces pericyte death, neurons are sacrificed in order to help prevent further degradation of the pericytes. Longer duration simulations outside the scope of this project would be useful to examine this theory, with adjustment of the values of c_{50} and c_5. This would help determine whether neuron health in Figure 5.17F can be made to plateau before full

death is seen, stabilising the $\hat{p}_t$, the pericyte health model and therefore allowing the model to reach a second complete steady state. This simulation indicates that in order to see the most rapid decay, pericyte death must significantly outpace neuron death, otherwise the neuron death will stabilise the response.

General discussion on the results

AB concentration has had a similar response in all cases. By setting the $\frac{dc}{dt}$ term equal to zero in Equation 4.13, the steady state value of c only depends on R and k:

$$c = \frac{R}{Q_{\text{norm}} + k} \tag{5.8}$$

As most simulations tend to zero flow rate and take default values of $R = 1$ and $k = 0.1$, the concentration often tends to $c_{ss} = 10$. After an initial constant period during baseline conditions, a hyperbolic tangent shaped response often connects the baseline condition and this final steady state value, which is formed due to a period of rapid c growth once a reduction in flow rate diminishes the clear-out of AB.

Another characteristic response of the results is a relatively large initial increase of V followed by a plateau and then decay for both pericytes and neurons. This is a consequence of the health models, where the rate of change from alive to vulnerable is proportional to the concentration of alive. The system starts with a maximum A value of one as an input, so the initial rate is high. Over time, as V increases, so does the rate of pericytes and neurons moving back towards the alive phase and also towards the dead phase. Movement to the dead phases is irreversible, so neither pericytes nor neurons will travel back to the vulnerable phase.

Numerical instability is seen in the simulations as the flow rate tends to zero, due to the rapid change in gradient of the Q_{norm} response. This is to be expected for a RK4 numerical scheme without sufficient smoothing. The greater the gradient of Q_{norm} as it approaches zero flow rate, the larger the instability. For the conditions investigated in this project, the instability has been minor and has not resulted in divergence.

5.3 Application to AD

The ultimate purpose of this model is to gain insight into the mechanisms linking AD and blood flow through quantitative modelling. This section will attempt to apply these results to AD behaviour, and offer new insights on the disease.

In the Literature Review section, it was suggested that pericyte death should occur rapidly once full ischaemia is reached, with one study showing that 90% of pericytes died within one hour of flow drop [52]. The results have, in fact, confirmed this. For example, 5.16 shows that once full ischaemia is reached, pericyte health collapses within a few hundred seconds. This model has a very similar response shape to the typical myogenic response in the literature, with a sharp rise in flow rate in response to the pressure difference, followed by acute adjustments and oscillations.

Pericyte health has been shown to be particularly important. Without any pericytes responding to the flow and constricting, the overall effects of the pericyte health model would be reduced. This confirms the hypothesis of the model – that pericyte constriction has an important role in AD pathology. The model has also demonstrated that pericyte health degradation in conjunction with its constriction response can lead to neuron health degradation. It has also shown that neuronal death may occur as a measure of protection of pericyte health.

Interestingly, in some cases, low flow rate actually restores neuron health. This is because the low flow rate allows the oxygen in the blood greater time to pass through the vessel wall into the tissue where it can rejuvenate the neurons.

While c and flow are important aspects of AD pathology, the neuronal degradation is the direct cause of the negative symptoms of AD. Though the system may appear healthier with higher flow rate, one must bear in mind that neuron health changes are just as important to track.

5.4 Conclusion

This section has presented the results for various combinations of inputs to the model. Most notably, it has shown that rapid death of the pericytes, combined with the pericyte response, greatly affects flow rate and AB accumulation. Furthermore, it has suggested that rapid neuron death may in fact protect the pericytes. Finally, it was shown that these results have physiological implications for AD.

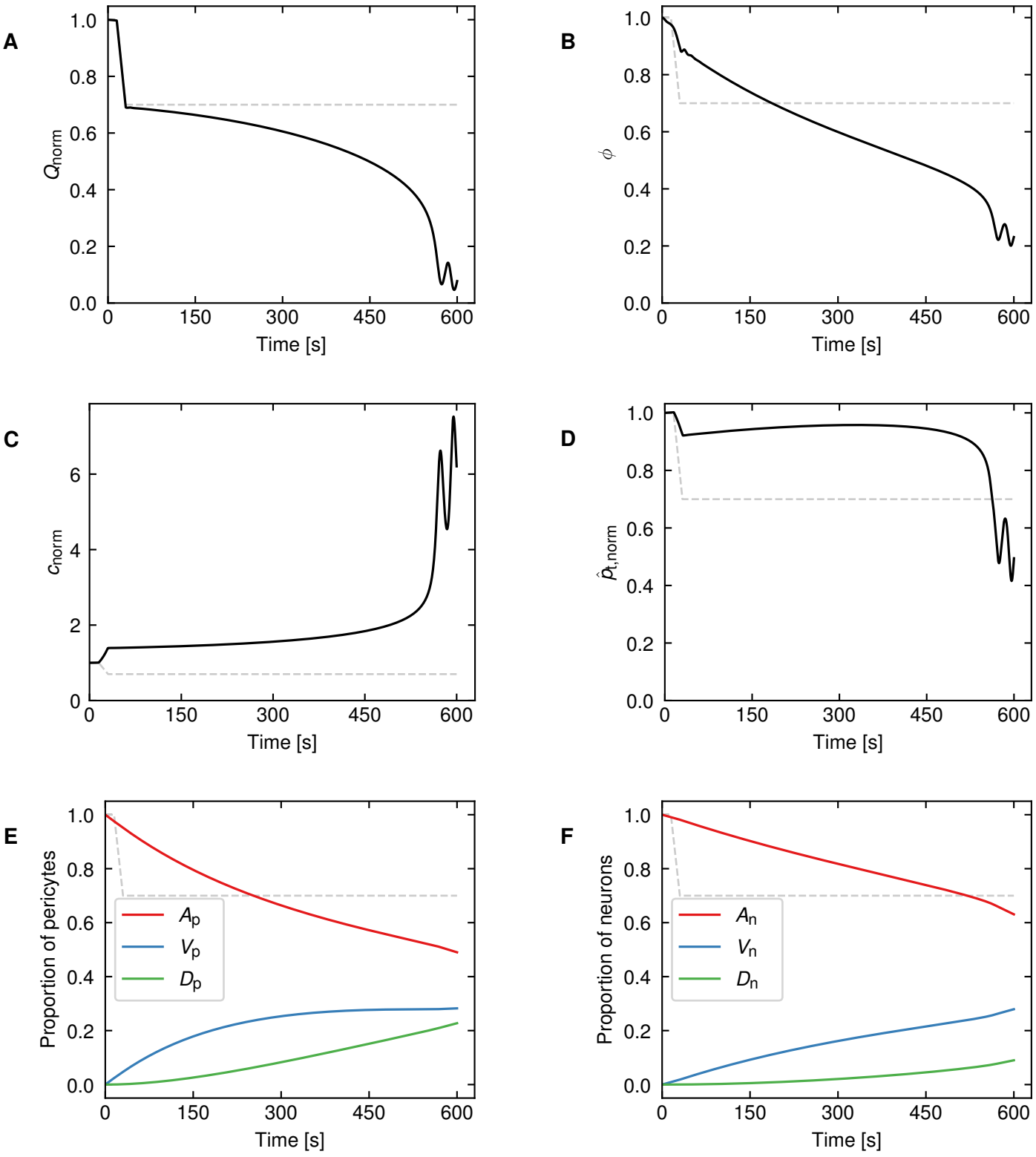

Figure 5.11: Default values results.
A: normalised flow rate response; **B**: ϕ response; **C**: normalised AB concentration response; **D**: $\hat{p}_t$ response; **E**: pericyte health model states; **F**: neuron health model states.

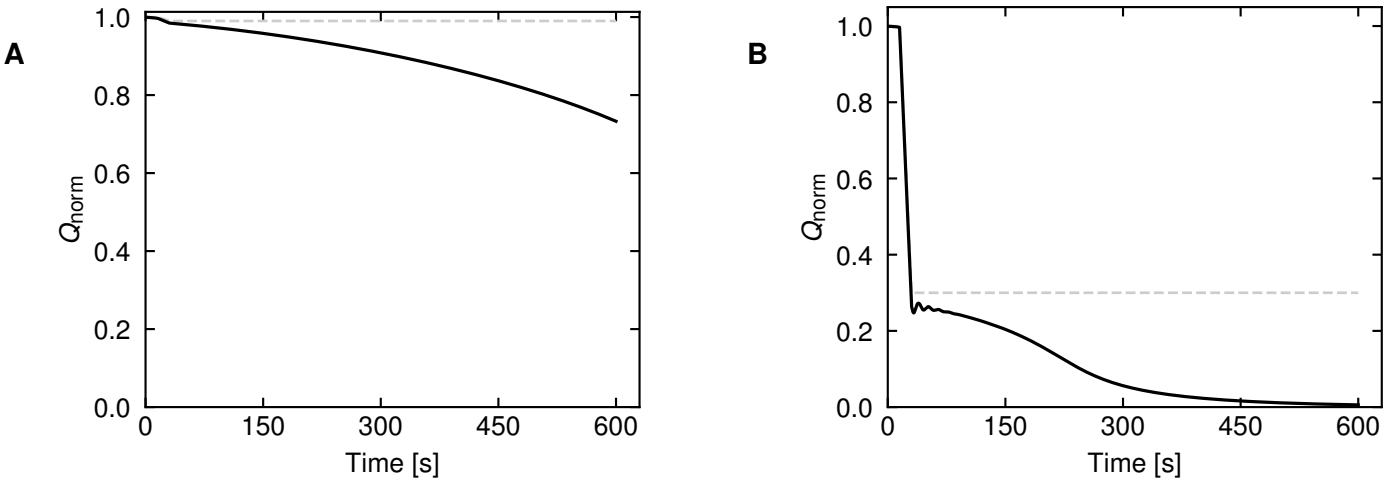

Figure 5.12: Comparing pressure drop values.
A: Flow rate plot for low pressure drop (0.01); **B**: Flow rate plot for high pressure drop (0.7).

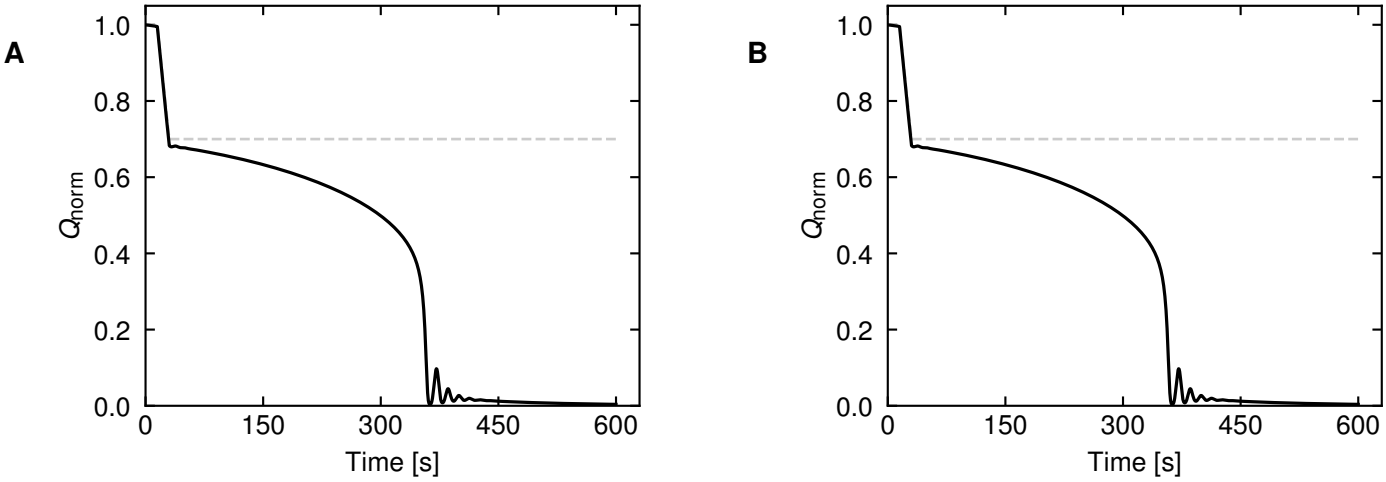

Figure 5.13: Comparing delay for α = 0.5.
A: Flow rate plot for low delay (0); **B**: Flow rate plot for high delay (7.62).

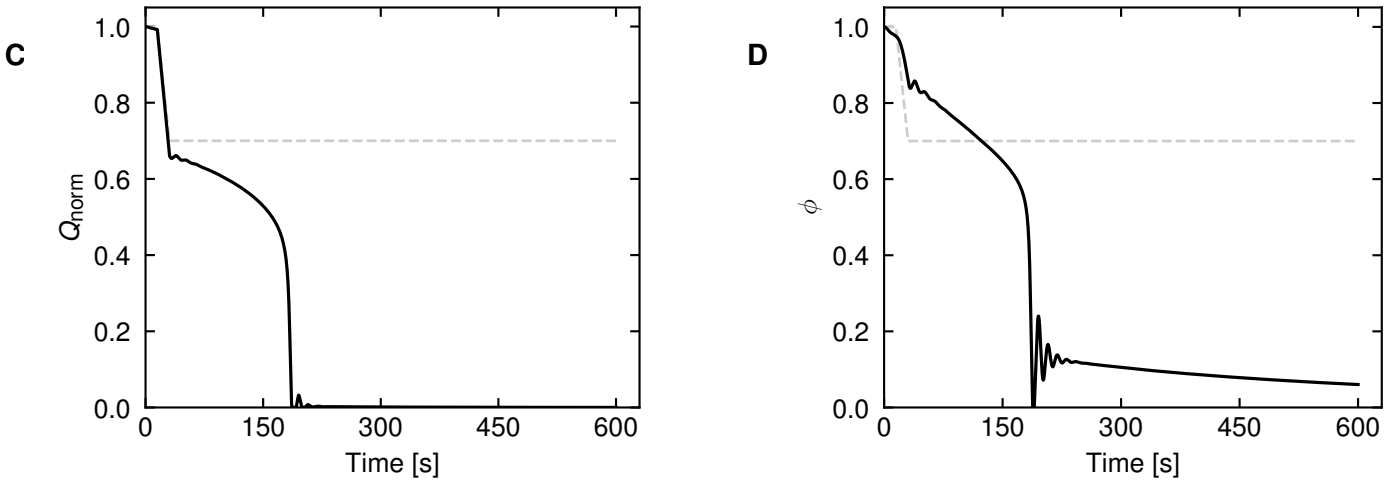

Figure 5.14: Showing high α results.
A: Flow rate plot for high alpha (0.9); **B**: ϕ plot for high alpha (0.9);

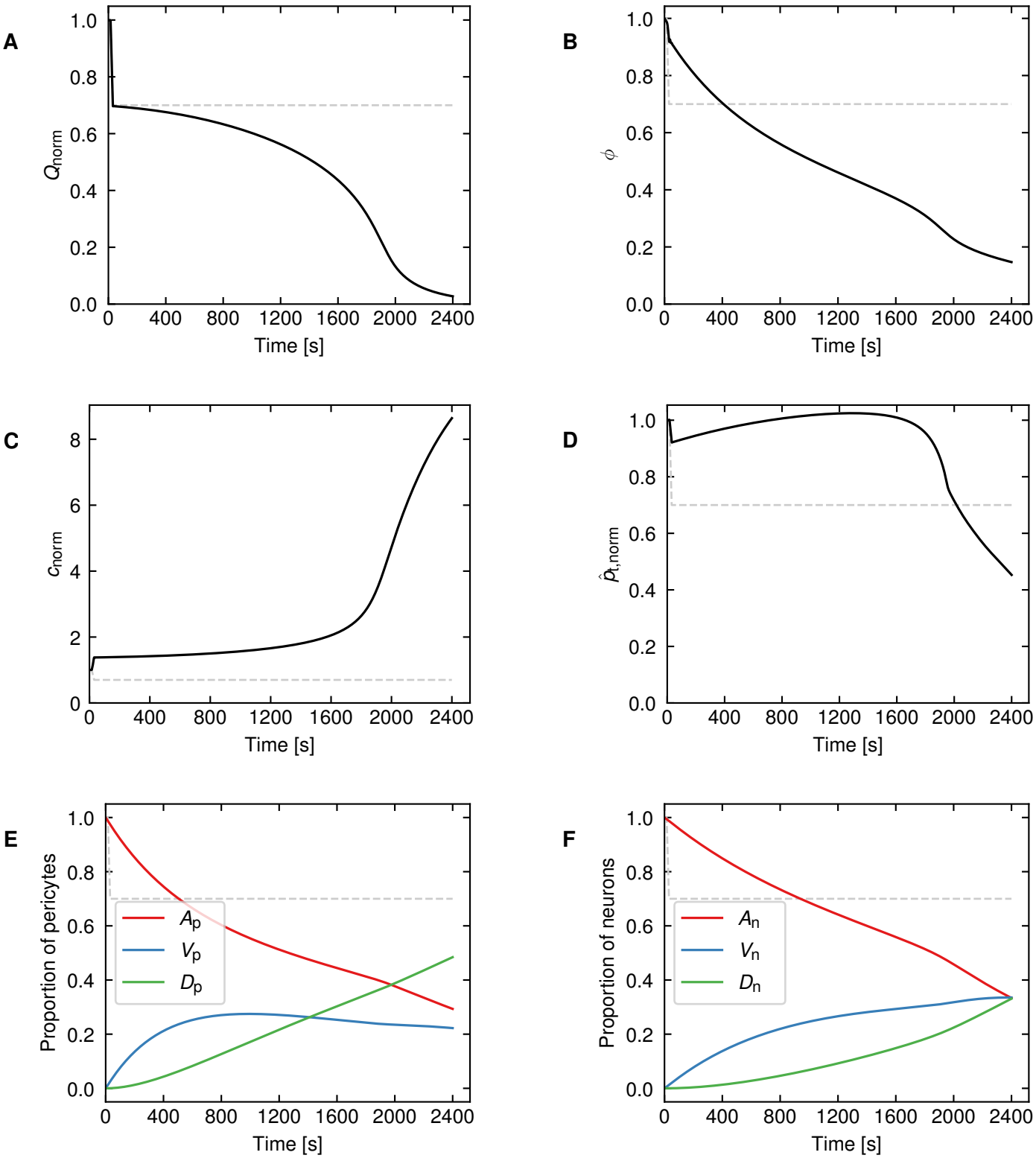

Figure 5.15: Slow response results..
A: normalised flow rate response; **B**: ϕ response; **C**: normalised AB concentration response; **D**: $\hat{p}_t$ response; **E**: pericyte health model states; **F**: neuron health model states.

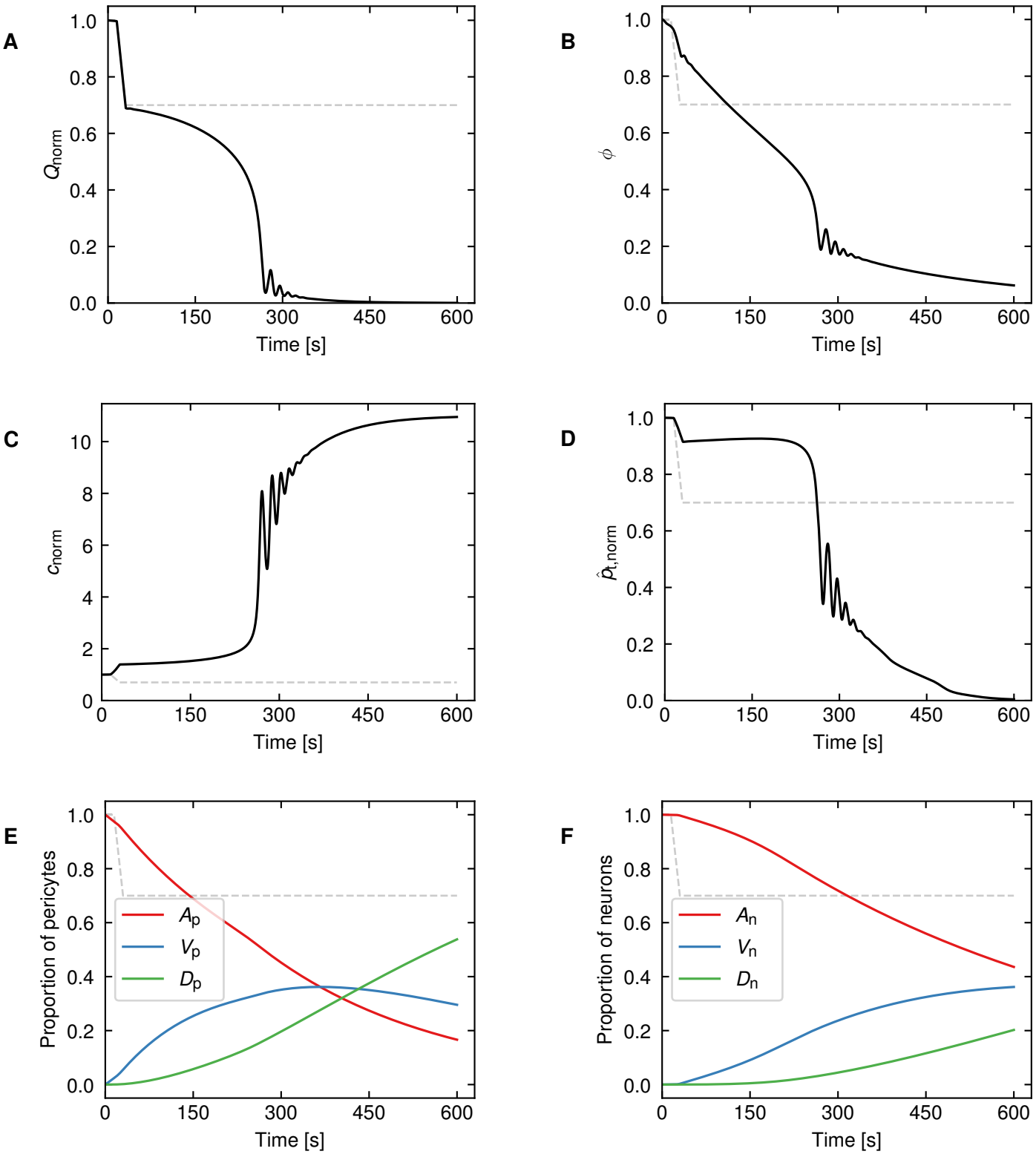

Figure 5.16: Accelerated response results..
A: normalised flow rate response; **B**: ϕ response; **C**: normalised AB concentration response; **D**: $\hat{p}_t$ response; **E**: pericyte health model states; **F**: neuron health model states.

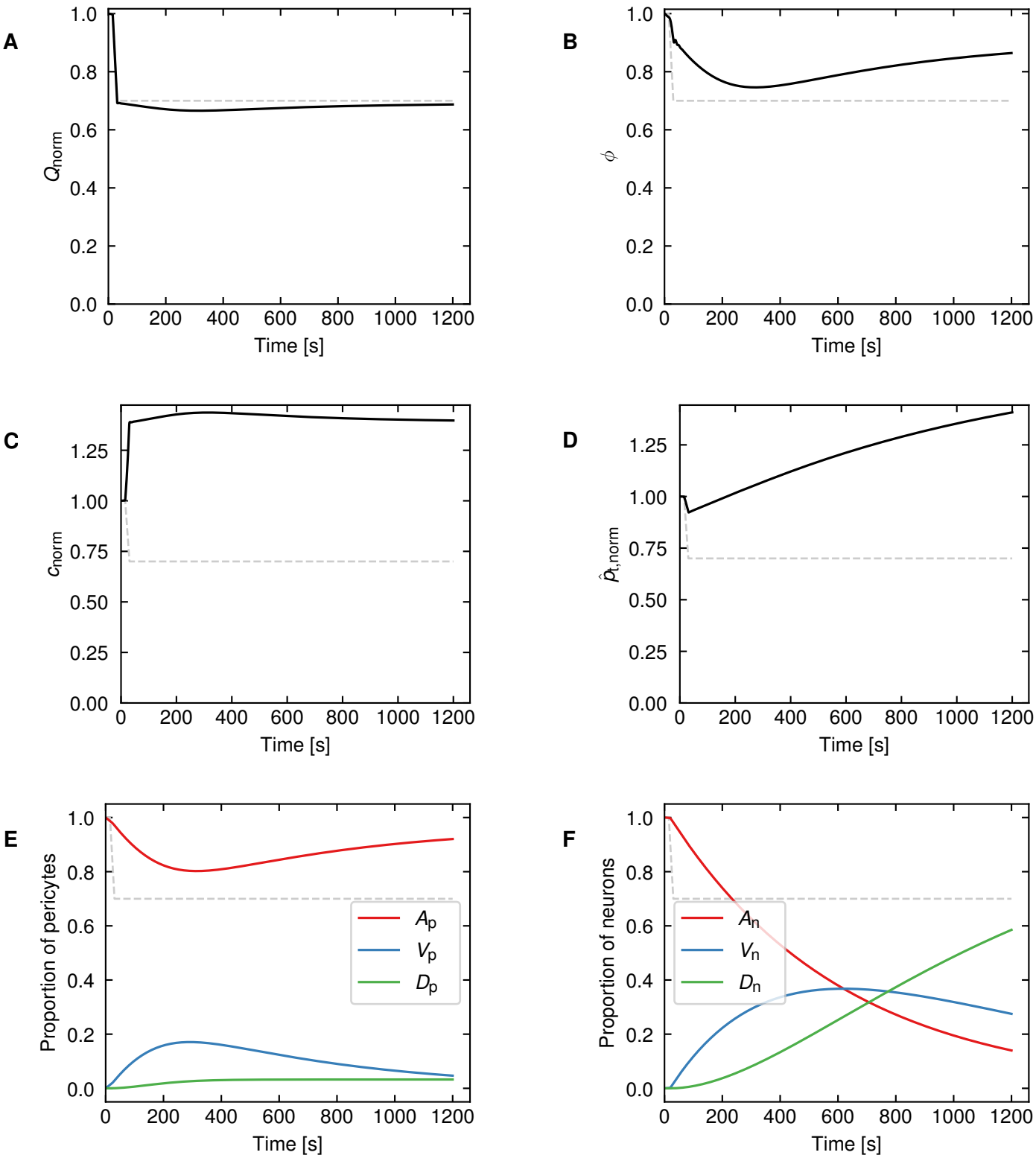

Figure 5.17: Second equilibrium results.
A: normalised flow rate response; **B**: ϕ response; **C**: normalised AB concentration response; **D**: $\hat{p}_t$ response; **E**: pericyte health model states; **F**: neuron health model states.

6 Project Discussion

The modification of an existing model of cerebral blood flow with a pericyte response has allowed for a quantitative understanding of how AB may accumulate and affect the health of the brain. Experimental data rendered possible the formation of a simple yet physiologically based control equation for the pericytes' constriction response to flow rate. The data have also allowed for the key values of this response to be extracted. The compartmental mass action kinetics style model of pericyte and neuron health has permitted modelling in an efficient computational manner and can effectively be fed back into the flow model. The hyperbolic tangent rate equations have proved particularly effective in terms of linking sensitivity of the flow and AB concentration to the health of the system.

The simplifications of the 1-D network and flow model have kept the run time for the longest simulations at an acceptable level, while short exploratory runs of 300 s took approximately 90 minutes. The RK4 model proved to be a sensible choice and made the application of the 44 ODEs manageable, while keeping run time low.

Due to the novelty of this approach, this model has not yet been validated by much experimental data. Despite this, results appear plausible given the shape of the response. The data that do exist have been useful in giving approximate values for the constants in the model. Experimenting within the suggested range for these constants has led to a wide range of responses. The model's modular nature has meant that it is possible to contrast and analyse these responses, validating them when the behaviour was expected, or modifying them when it was not.

It has been established that pericyte death is a key feature of this model, strengthening the project's hypothesis that pericytes have a vital role in AB accumulation and AD onset. The model has shown that initial rapid neuron death both stabilises blood flow longer and maintains pericyte health longer by decreasing the tissue metabolism.

Assumptions and limitations

The assumptions and limitations of this project arise due to three main reasons: computational resource constraints, time constraints and a lack of experimental data in the literature.

The limitations of computational resources have meant that various assumptions and approximations had to be made in order to keep run times low and allow for the consideration of many combinations of inputs. Discrete application of constriction on capillaries was an option, but a weighted average was performed instead to update the capillary segment resistance. To prioritise a wide spread of simulation

constant combinations, few longer duration runs were able to be performed.

Beyond computational constraints, some models were chosen due to their relatively straight simple interpretation. This involved some trade-offs, for example, the health models were limited insofar as they treat all pericytes and neurons as being in discrete compartments. In reality, pericytes and neurons gradually transition from a state of good health to one of poor health. Additionally, the health models were connected to the flow model only using the proportion of 'alive'. The assumption that capillary diameter is based on flow rate ignores the nuance of the complex signalling pathways and neurotransmitters that would actually perform this process. An independent and constant tissue compartment for each vessel is assumed, when in fact, the compartments are likely to overlap, and the oxygen will not be perfectly contained.

The greatest challenge to this project is probably the lack of sufficient experimental data. This would enable the formation of more detailed and accurate modelling methods. Furthermore, where data have been found, they have often not been corroborated by other studies. The ODEs controlling the model have supported the yield of interesting results, but there is not a wide range of data in the limited literature to ground them. In particular, there are insufficient data on the pericyte' response, as well as a lack of understanding on the mechanisms behind AB accumulation. Both of these issues stem from the problems of imaging in vivo inside the skull. This shortage of data in terms of the pericyte response to flow conditions other than full ischaemia led to the use of linear interpolation. A small change in this distribution would strongly affect the results of the model. Here, the assumption is that pericytes, and not arterioles, relax, but this is far from certain given that the literature is divided on this topic. Some data to allow comparison against this AB accumulation model would be helpful for developing a more detailed model. The pericyte response to flow which forms the basis of our pericyte response model assumed that capillaries are any blood vessel of diameter below 10 µm [52]. In our network model, the A5 and A6 arteriole segments also have diameters sub 10 µm.

There are further issues relating to the model and the modelling decisions made. The instability of the system to certain ranges of the delay when paired with other values prevents a complete analysis of this delay. The time constants explored in this project are also considerably lower than would be seen in human AD sufferers, in part due to computational and time constraints, but a more tailored numerical solver would allow for a more realistic time frame. In this model, the ϕ value can and does fall below 0.153 with high pericyte death, despite experimental data suggesting 0.153 is the average constriction of dead pericytes [52].

7 Conclusion

This project sought to explore new potential causes of AD. Informed by experimental data, a delayed ODE pericyte response model was created, which constricted the capillaries depending on the level of blood flow rate into the vessel. A further ODE was formed to model the accumulation of AB in the tissue. Additionally, neuron and pericyte health models were created in a mass action kinetics style to monitor the health of the brain. Due to its toxicity, the concentration of AB was assumed to affect the neuron health model. This model was joined into the flow model by scaling the metabolism of the tissue by the proportion of alive neurons. The pericyte health model was based on the oxygenation of the tissue and joined the flow model by limiting the response of the pericyte.

In the results section, each of these units was first introduced individually to ensure that their exhibited response was plausible, and to shed light on the units' effect on the full model response. Characteristic results of the full model were then presented. These demonstrated the relative importance of different input values and highlighted the most important mechanisms in the flow response. In this model, pericyte constriction has been found to vastly affect the mode and magnitude of the system response, suggesting that pericytes and blood flow do indeed have an impact on AD onset and pathology, advocating the need for further research.

Areas for Development

The model development process and results of this project have brought to light certain areas for development. Disagreement persists on whether it is the pericyte, the arterioles or, more likely, a combination of them that contract. Developing the model to include upstream propagation and the effect of the contraction signal from the capillary to arterioles may produce interesting and more extreme results. Other responses, such as the hemodynamic or autoregulatory responses, could be built into the model to see how these affect the stability of AB concentration and help prevent the death of pericytes and neurons. The current input to the system of a ramped pressure drop has proved to be a successful way to investigate the model response. However, more complex input models for pressure combined with other values may reveal different responses not found within the scope of this project. Hallmarks of AD, such as AB accumulation and hypoperfusion, have been observed in patients as early as 25 years pre symptoms. A solver modified for the stiff nature of this model would allow simulations that explore longer durations.

References

[1] S. J. Payne and C. Lucas, "Oxygen delivery from the cerebral microvasculature to tissue is governed by a single time constant of approximately 6 seconds," *Microcirculation*, vol. 25, no. 2, pp. 1–11, 2018.

[2] Mathers C., G. Stevens, Mahanani W.R., D. Fat, and D. Hogan, "WHO — Disease burden and mortality estimates," Tech. Rep. March, 2018, pp. 1–65.

[3] World Health Organisation, "Global action plan on the public health response to dementia 2017 - 2025," *Geneva: World Health Organization*, p. 52, 2017.

[4] M. Prince, A. Wimo, M. Guerchet, A. Gemma-Claire, Y.-T. Wu, and M. Prina, "World Alzheimer Report 2015: The Global Impact of Dementia - An analysis of prevalence, incidence, cost and trends," *Alzheimer's Disease International*, p. 84, 2015.

[5] M. Prince, M. Knapp, *et al.*, "Dementia UK: Update Second edition," Tech. Rep., 2014, pp. viii–xii.

[6] D. F. Weaver, "The impending alzheimer's disease pandemic," *University of Toronto Medical Journal*, vol. 95, no. 2, pp. 6–7, 2018.

[7] A. Wimo, M. Guerchet, *et al.*, "The worldwide costs of dementia 2015 and comparisons with 2010," *Alzheimer's and Dementia*, vol. 13, no. 1, pp. 1–7, Jan. 2017.

[8] Office for National Statistics, "Leading causes of death, UK: 2001 to 2018," Table 5, 2020.

[9] Alzheimer's Disease International, "Policy Brief for Heads of Government: The Global Impact of Dementia 2013–2050," Tech. Rep., 2013.

[10] J. Jebelli, *In Pursuit of Memory: The Fight Against Alzheimer's*. John Murray, 2017.

[11] D. M. Bagad, D. Chowdhury, and Z. Khan, "Towards understanding Alzheimer's Disease: An Overview," *Research Journal of Pharmaceutical, Biological and Chemical Sciences*, vol. 4, pp. 286–298, 2013.

[12] R. J. O'Brien and P. C. Wong, "Amyloid precursor protein processing and Alzheimer's disease.," eng, *Annual review of neuroscience*, vol. 34, pp. 185–204, 2011.

[13] W. F. Goure, G. A. Krafft, J. Jerecic, and F. Hefti, "Targeting the proper amyloid-beta neuronal toxins: a path forward for Alzheimer's disease immunotherapeutics," *Alzheimer's Research & Therapy*, vol. 6, no. 4, p. 42, 2014.

[14] A. G. W. van Norden, E. J. van Dijk, K. F. de Laat, P. Scheltens, M. G. M. Olderikkert, and F. E. de Leeuw, "Dementia: Alzheimer pathology and vascular factors: from mutually exclusive to interaction.," eng, *Biochimica et biophysica acta*, vol. 1822, no. 3, pp. 340–349, Mar. 2012.

[15] R. Luengo-Fernandez, J. Leal, and A. Gray, "UK research spend in 2008 and 2012: comparing stroke, cancer, coronary heart disease and dementia.," eng, *BMJ open*, vol. 5, no. 4, e006648, Apr. 2015.

[16] F. Kametani and M. Hasegawa, “Reconsideration of Amyloid Hypothesis and Tau Hypothesis in Alzheimer’s Disease.,” eng, *Frontiers in neuroscience*, vol. 12, p. 25, 2018.

[17] F. Hyder, D. L. Rothman, and M. R. Bennett, “Cortical energy demands of signaling and nonsignaling components in brain are conserved across mammalian species and activity levels,” *Proceedings of the National Academy of Sciences*, vol. 110, no. 9, 3549 LP –3554, Feb. 2013.

[18] S. B. Heymsfield, T. Chirachariyavej, I. J. Rhyu, C. Roongpisuthipong, M. Heo, and A. Pietrobelli, “Differences between brain mass and body weight scaling to height: potential mechanism of reduced mass-specific resting energy expenditure of taller adults,” eng, *Journal of applied physiology (Bethesda, Md. : 1985)*, vol. 106, no. 1, pp. 40–48, Jan. 2009.

[19] C. Iadecola, “The pathobiology of vascular dementia.,” eng, *Neuron*, vol. 80, no. 4, pp. 844–866, Nov. 2013.

[20] J. A. Schneider, Z. Arvanitakis, W. Bang, and D. A. Bennett, “Mixed brain pathologies account for most dementia cases in community-dwelling older persons,” *Neurology*, vol. 69, no. 24, 2197 LP –2204, Dec. 2007.

[21] J. B. Toledo, S. E. Arnold, *et al.*, “Contribution of cerebrovascular disease in autopsy confirmed neurodegenerative disease cases in the National Alzheimer’s Coordinating Centre.,” eng, *Brain : a journal of neurology*, vol. 136, no. Pt 9, pp. 2697–2706, Sep. 2013.

[22] J. Attems and K. A. Jellinger, “The overlap between vascular disease and Alzheimer’s disease–lessons from pathology.,” eng, *BMC medicine*, vol. 12, p. 206, Nov. 2014.

[23] M. Pase, C. L. Satizabal, and SeshadriSudha, “Role of Improved Vascular Health in the Declining Incidence of Dementia,” *Stroke*, vol. 48, no. 7, pp. 2013–2020, Jul. 2017.

[24] R. F. Gottesman, A. L. C. Schneider, *et al.*, “Association Between Midlife Vascular Risk Factors and Estimated Brain Amyloid Deposition.,” eng, *JAMA*, vol. 317, no. 14, pp. 1443–1450, Apr. 2017.

[25] L. J. Launer, G. Ross, *et al.*, “Midlife blood pressure and dementia: the Honolulu–Asia aging study,” *Neurobiology of Aging*, vol. 21, no. 1, pp. 49–55, 2000.

[26] D. Carnevale, G. Mascio, *et al.*, “Hypertension induces brain beta-amyloid accumulation, cognitive impairment, and memory deterioration through activation of receptor for advanced glycation end products in brain vasculature.,” eng, *Hypertension (Dallas, Tex. : 1979)*, vol. 60, no. 1, pp. 188–197, Jul. 2012.

[27] C. Y. Santos, P. J. Snyder, W.-C. Wu, M. Zhang, A. Echeverria, and J. Alber, “Pathophysiologic relationship between Alzheimer’s disease, cerebrovascular disease, and cardiovascular risk: A review and synthesis.,” eng, *Alzheimer’s & dementia (Amsterdam, Netherlands)*, vol. 7, pp. 69–87, 2017.

[28] I. Broce, C. M. Karch, *et al.*, “Immune-related genetic enrichment in frontotemporal dementia: An analysis of genome-wide association studies.,” eng, *PLoS medicine*, vol. 15, no. 1, e1002487, Jan. 2018.

[29] R. J. Bateman, C. Xiong, *et al.*, “Clinical and Biomarker Changes in Dominantly Inherited Alzheimer’s Disease,” *New England Journal of Medicine*, vol. 367, no. 9, pp. 795–804, Jul. 2012.

[30] T. Thomas, S. Miners, and S. Love, “Post-mortem assessment of hypoperfusion of cerebral cortex in Alzheimer’s disease and vascular dementia.,” eng, *Brain : a journal of neurology*, vol. 138, no. Pt 4, pp. 1059–1069, Apr. 2015.

[31] K. Kisler, A. R. Nelson, A. Montagne, and B. V. Zlokovic, “Cerebral blood flow regulation and neurovascular dysfunction in Alzheimer disease.,” eng, *Nature reviews. Neuroscience*, vol. 18, no. 7, pp. 419–434, Jul. 2017.

[32] A. Ezzati, C. Wang, *et al.*, “Association Between Vascular Pathology and Rate of Cognitive Decline Independent of Alzheimer’s Disease Pathology,” *Journal of the American Geriatrics Society*, vol. 65, no. 8, pp. 1836–1841, Aug. 2017.

[33] F. Arba, G. Mair, *et al.*, “Cerebral White Matter Hypoperfusion Increases with Small-Vessel Disease Burden. Data From the Third International Stroke Trial.,” eng, *Journal of stroke and cerebrovascular diseases : the official journal of National Stroke Association*, vol. 26, no. 7, pp. 1506–1513, Jul. 2017.

[34] M. R. Azarpazhooh, A. Avan, L. E. Cipriano, D. G. Munoz, L. A. Sposato, and V. Hachinski, “Concomitant vascular and neurodegenerative pathologies double the risk of dementia.,” eng, *Alzheimer’s & dementia : the journal of the Alzheimer’s Association*, vol. 14, no. 2, pp. 148–156, Feb. 2018.

[35] H. J. Kim, K. Im, *et al.*, “Effects of amyloid and small vessel disease on white matter network disruption.,” eng, *Journal of Alzheimer’s disease : JAD*, vol. 44, no. 3, pp. 963–975, 2015.

[36] I. Costantino and G. R. F., “Cerebrovascular Alterations in Alzheimer Disease,” *Circulation Research*, vol. 123, no. 4, pp. 406–408, Aug. 2018.

[37] C. Iadecola, “The Neurovascular Unit Coming of Age: A Journey through Neurovascular Coupling in Health and Disease,” *Neuron*, vol. 96, no. 1, pp. 17–42, Sep. 2017.

[38] A. Liesz, “The vascular side of Alzheimer's disease,” *Science*, vol. 365, no. 6450, 223 LP –224, Jul. 2019.

[39] E. Zenaro, G. Piacentino, and G. Constantin, “The blood-brain barrier in Alzheimer’s disease.,” eng, *Neurobiology of disease*, vol. 107, pp. 41–56, Nov. 2017.

[40] A. Charidimou, G. Boulouis, *et al.*, “Emerging concepts in sporadic cerebral amyloid angiopathy,” *Brain*, vol. 140, no. 7, pp. 1829–1850, Mar. 2017.

[41] C. M. Peppiatt, C. Howarth, P. Mobbs, and D. Attwell, “Bidirectional control of CNS capillary diameter by pericytes,” *Nature*, vol. 443, no. 7112, pp. 700–704, 2006.

[42] F. M. O’Farrell, S. Mastitskaya, M. Hammond-Haley, F. Freitas, W. R. Wah, and D. Attwell, “Capillary pericytes mediate coronary no-reflow after myocardial ischaemia.,” eng, *eLife*, vol. 6, Nov. 2017.

[43] R. Nortley, N. Korte, *et al.*, “Amyloid beta oligomers constrict human capillaries in Alzheimer’s disease via signaling to pericytes.,” eng, *Science (New York, N.Y.)*, vol. 365, no. 6450, Jul. 2019.

[44] M. W. Ma, J. Wang, *et al.*, “NADPH oxidase in brain injury and neurodegenerative disorders,” eng, *Molecular neurodegeneration*, vol. 12, no. 1, p. 7, Jan. 2017.

[45] F. Cassot, F. Lauwers, C. Fouard, S. Prohaska, and V. Lauwers-Cances, “A novel three-dimensional computer-assisted method for a quantitative study of microvascular networks of the human cerebral cortex.,” eng, *Microcirculation (New York, N.Y. : 1994)*, vol. 13, no. 1, pp. 1–18, Jan. 2006.

[46] S. Lorthois, F. Cassot, and F. Lauwers, “Simulation study of brain blood flow regulation by intra-cortical arterioles in an anatomically accurate large human vascular network: Part I: methodology and baseline flow.,” eng, *NeuroImage*, vol. 54, no. 2, pp. 1031–1042, Jan. 2011.

[47] Y. Shi, P. Lawford, and R. Hose, “Review of Zero-D and 1-D Models of Blood Flow in the Cardiovascular System,” *BioMedical Engineering OnLine*, vol. 10, no. 1, p. 33, 2011.

[48] J. B. Mandeville, J. J. Marota, *et al.*, “Evidence of a cerebrovascular postarteriole windkessel with delayed compliance.,” eng, *Journal of cerebral blood flow and metabolism : official journal of the International Society of Cerebral Blood Flow and Metabolism*, vol. 19, no. 6, pp. 679–689, Jun. 1999.

[49] R. B. Buxton, L. R. Frank, E. C. Wong, B. Siewert, S. Warach, and R. R. Edelman, “A general kinetic model for quantitative perfusion imaging with arterial spin labeling,” *Magnetic Resonance in Medicine*, vol. 40, no. 3, pp. 383–396, Sep. 1998.

[50] R. D. Freeman and B. Li, “Neural-metabolic coupling in the central visual pathway.,” eng, *Philosophical transactions of the Royal Society of London. Series B, Biological sciences*, vol. 371, no. 1705, Oct. 2016.

[51] D. Attwell, A. M. Buchan, S. Charpak, M. Lauritzen, B. A. Macvicar, and E. A. Newman, “Glial and neuronal control of brain blood flow.,” eng, *Nature*, vol. 468, no. 7321, pp. 232–243, Nov. 2010.

[52] C. N. Hall, C. Reynell, *et al.*, “Capillary pericytes regulate cerebral blood flow in health and disease.,” eng, *Nature*, vol. 508, no. 7494, pp. 55–60, Apr. 2014.

[53] E. W. Washburn, “The Dynamics of Capillary Flow,” *Physical Review*, vol. 17, no. 3, pp. 273–283, Mar. 1921.

[54] J. W. Severinghaus, “Blood gas calculator.,” *Journal of applied physiology*, vol. 21, no. 3, pp. 1108–1116, 1966.

Appendices

A Constant values

Symbol	Name	Value and Units
α_t	Solubility coefficient of oxygen in brain tissue	$2.6 \times 10^{-5}\,\mathrm{mL_{O2}mL^{-1}mmHg^{-1}}$
K	Oxygen permeability of vascular wall	$5 \times 10^{-2}\,\mu\mathrm{m^2 s^{-1} mmHg^{-1}}$
c_{Hb}	Oxygen-carrying capacity per unit volume of red blood cells	$0.2\,\mathrm{mL_{O2}mL^{-1}}$
H	Hematocrit	0.42
M_{const}	Oxygen consumption of tissue per unit volume	$8.20 \times 10^{-4}\,\mathrm{cm^3_{O2} cm^{-3} s^{-1}}$
θ	Hill equation constant	2 mmHg
ϕ_{FI}	Minimum normal diameter of capillary in response to full ischaemia	0.153
τ_{p}	Pericyte response time constant	$2.29\,\mathrm{s^{-1}}$
$\bar{p}_{\mathrm{a}}$	Baseline arteriolar blood pressure	60mmHg
p_{v}	Venous blood pressure	15mmHg

B Network Parameters at baseline

Branch	Number of vessels	Diamater µm	Length µm	Wall thickness m	Viscosity µmmHgs
A1	1	23.97	1267.6	4.84	11.9
A2	2	19.17	930.3	4.25	11.3
A3	4	15.28	543.6	3.81	10.7
A4	8	12.08	302.3	3.49	10.1
A5	16	9.46	161.2	3.27	9.6
A6	32	7.32	154.7	3.14	9.2
C	64	8.00	243.9	3.17	9.3
V6	32	11.51	473.9	3.43	10.0
V5	16	14.53	272.3	3.73	10.5
V4	8	17.79	426.6	4.09	11.1
V3	4	21.45	632.5	4.53	11.6
V2	2	25.7	844.2	5.06	12.2
V1	1	30.77	936.3	5.72	12.8

C Default model inputs

Parameter:	τ_{d}	α	p_{drop}	c_{50}	c_5	$\hat{p}_{\mathrm{t},50}$	$\hat{p}_{\mathrm{t},5}$	$k_{\mathrm{n,const}}$	$k_{\mathrm{p,const}}$	τ_{c}	R	k
Default Value:	7.62	0.3	0.3	$2.6\overline{c}$	$2\overline{c}$	$1\hat{p}_{\mathrm{t}}$	$2\hat{p}_{\mathrm{t}}$	1/300	1/600	1/600	1	0.1